Surface circulation in the Gulf of Cadiz:
Model and mean flow structure

Alvaro Peliz,[1] Jesus Dubert,[1] Patrick Marchesiello,[2] and Ana Teles-Machado[1]

[1]   The mean flow structure of the Gulf of Cadiz is studied using a numerical model. The model consists of a set of one-way nested configurations attaining resolutions on the order of 2.6 km in the region of the Gulf of Cadiz. In the large-scale configuration, the entrainment of the Mediterranean Water is parameterized implicitly through a nudging term. In medium- and small-scale nested configurations, the Mediterranean outflow is introduced explicitly. The model reproduces all the known features of the Azores Current and of the circulation inside the Gulf of Cadiz. A realistic Mediterranean Undercurrent is generated and Meddies develop at proper depths on the southwest tip of the Iberian slope. The hypothesis that the Azores Current may generate in association with the Mediterranean outflow (β-plume theories) is confirmed by the model results. The time-mean flow is dominated by a cyclonic cell generated in the gulf which expands westward and has transports ranging from 4 to 5 Sv. The connection between the cell and the Azores Current is analyzed. At the scale of the Gulf, the time-mean flow cell is composed by the westward Mediterranean Undercurrent, and by a counterflow running eastward over the outer edge of the Mediterranean Undercurrent deeper vein, as the latter is forced downslope. This counterflow feeds the entrainment at the depths of the Mediterranean Undercurrent and the Atlantic inflow at shallower levels. Coastward and upslope of this recirculation cell, a second current running equatorward all the way along the northern part of the gulf is revealed. This current is a very robust model result that promotes continuity between the southwestern Iberian coast and the Strait of Gibraltar, and helps explain many observations and recurrent SST features of the Gulf of Cadiz.

1. Introduction

[2]   The Gulf of Cadiz in the northeastern Atlantic is one of the most complex and interesting circulation spots in the world ocean. On the one hand, it constitutes the zone of exchange with the Mediterranean sea through the Strait of Gibraltar, and the Mediterranean inflow/outflow strongly influences the local circulation, particularly owing to the generation of the intermediate depth Mediterranean Undercurrent (MU) and Mediterranean water eddies (Meddies) [e.g., *Ambar and Howe*, 1979; *Serra and Ambar*, 2002; *Baringer and Price*, 1997a, 1997b]. On the other hand, the summer season is characterized by strongly stratified upper layer and the intensification of northerlies with the consequent development of upwelling like features (jets and filaments) along the west coast of Iberia. The abrupt change in coastline orientation and the presence of the strait connecting two very different basins favors the generation

of heterogeneous wind fields, jet separation and coastal counter currents [*Folkard et al.*, 1997; *Relvas and Barton*, 2002, 2005; *Sánchez et al.*, 2006; *Sánchez and Relvas*, 2003; *Garcia-Lafuente et al.*, 2006]; Finally, concerning the extracoastal dynamics, the Gulf of Cadiz is still under the influence of the eastern end of the Azores Current (AzC), since the eastward transports near the Gulf are still significant [*Arhan et al.*, 1994; *Paillet and Mercier*, 1997; *Peliz et al.*, 2005].

[3]   Recent studies challenge the classic understanding of the Azores Current by showing that a zonal cyclonic recirculation may be generated in response to entrainment of Atlantic Central Water by the Mediterranean Undercurrent. This recirculation could then explain the AzC and the Azores Countercurrent (AzCC) [*Jia*, 2000; *Özgökmen et al.*, 2001; *Kida*, 2006]. These studies (that we will refer to as β-plume models for short) support the generation of the Azores Current in the Gulf of Cadiz, but show significantly different AzC transport values. Also, they do not explain the observational evidence that the AzC transports are higher in the western part (at the longitude of Azores Islands) than in the east.

[4]   A serious shortcoming of existing models exploring the β-plume theory is that the main forcing factor, the

---

[1]Centro de Estudos do Ambiente e do Mar (CESAM), Departamento de Física, Universidade de Aveiro, Aveiro, Portugal.
[2]Institut de Recherche pour le Développement, Noumea, New Caledonia.

entrainment of the Central Water by the MU, is based on very simple parameterizations. The various scales involved, the forcing and uniqueness of the Gibraltar Strait exchange processes have precluded the development of regional-scale, realistic, high-resolution numerical models of this region. Realistic Mediterranean Undercurrent representation in the models requires horizontal scales on the order of 2 km with dense vertical resolutions [*Serra et al.*, 2005]. On the other hand, the Azores current is a cross-Atlantic zonal jet noticeable from the Gulf of Cadiz to at least the Mid-Atlantic Ridge. Therefore its simulation requires a relatively large computational domain.

[5] The objective of the present work is to achieve numerical solutions for the Gulf of Cadiz using nested configurations where the main large- and small-scale processes are represented. The ultimate goal is to understand how the β-plume mechanism develops in more realistic conditions and how the circulation at the scale of the Gulf of Cadiz couples with the Azores Current. The approach is to use large-scale configurations where the Mediterranean Water effects are parameterized, as boundary conditions for higher-resolution nested grids, where the exchange with the Mediterranean is explicitly represented.

[6] The present paper concentrates on the time-mean flow structure. The response to atmospheric synoptic variability will be addressed elsewhere.

[7] A short introduction to β-plume models is noteworthy. *Kida* [2006] revises the β-plume theory and its application to the Azores Current. The vorticity equation

$$\beta v = \frac{f_0 w^*}{h} + A_H \nabla^2 \zeta \qquad (1)$$

holds for a steady vertically integrated flow in a basin-scale context [*Stommel*, 1982; *Pedlosky*, 1997], where β is the meridional gradient of the Coriolis parameter f_0, w^* stands for the diapycnal velocity, h the water column height, and the term $A_H \nabla^2 \zeta$ stands for the viscous dissipation of the relative vorticity. This equation states that for a given latitude, a mass sink in a given layer (or a change in the water column $f_0 w^*/h$) should be compensated by a source at the same latitude or by the dissipative term $A_H \nabla^2 \zeta$. The zonal flow results from a vorticity balance between the sink and the source of vorticity. In the case of the Gulf of Cadiz, the sink in the upper layer is provided by the entrainment induced by mixing with the Mediterranean Undercurrent water.

[8] In what concerns the transport, the zonal flow/mass sink ratio (V/W) scales as $f_0/\beta L_y$, where L_y represents the meridional dimension of the sink zone. Simple calculations show that in this vorticity balance the zonal flow transport is 2 orders of magnitude larger than that of the sink; that is, for 1 Sv of entrainment the zonal flow is on the order of 100 Sv. This value is not realistic in the case of AzC. However, if in equation (1), β stands for background topographic vorticity instead of planetary vorticity, then the scaling predicts 2 Sv of horizontal circulation for 1 Sv of entrainment. This ratio is closer but below the reality of the AzC.

[9] *Kida* [2006] further develops the theory using a two layer framework, and arrives to an equation for the Reynolds decomposed potential vorticity ($q = \bar{q} + q'$) of a given layer,

$$\bar{U} \cdot \nabla \bar{q} = \bar{q} w^* - \nabla \cdot \overline{(U'q')} + \hat{k} \cdot \nabla \times \bar{F}. \qquad (2)$$

[10] In an inviscid context, the advection of vorticity is balanced by the entrainment factor ($\bar{q} w^*$), and by an additional term associated with the eddy potential vorticity fluxes ($\nabla \cdot \overline{(U'q')}$). This equation holds for an along slope overflow like the Mediterranean Undercurrent. The numerical experiments of *Kida* [2006] have demonstrated that these dynamics can develop a surface transport of about 4 Sv associated with entrainment and eddy fluxes, that *Kida* [2006] termed the topographic β plume.

[11] The outline of the paper is as follows. The next two sections is devoted to the model and methods. The results of the large-scale experiments are described in section 4. Section 5 briefly describes the Mediterranean Undercurrent in the model results. In section 6, the mean flow structure in the Gulf of Cadiz is analyzed. A discussion and comparison with previous studies is presented in section 7, followed by a conclusion.

2. Numerical Model

[12] The ocean simulations were performed using the Regional Oceanic Modelling System (ROMS) described by *Shchepetkin and McWilliams* [2003, 2005]. ROMS is a 3D free-surface, sigma-coordinate, split-explicit primitive equation model with Boussinesq and hydrostatic approximations. The finite-difference discretization algorithms are orientated toward nonoscillatory high-order schemes, thus improving the effective resolution of the model. In particular, a third-order, upstream-biased advection scheme with implicit lateral diffusion allows the generation of steep gradients, while a new pressure gradient algorithm ensures low levels of sigma-related errors. A third-order accurate predictor-corrector-leapfrog/Adams-Moulton−time step algorithm is used which allows a substantial increase of time step as well as good dispersive properties for the advection equation. The open boundary conditions are, for the baroclinic mode, a combination of outward radiation and flow-adaptive nudging toward prescribed external conditions, and for the barotropic mode a Flather-type condition to ensure well-posed tidal forcing [*Marchesiello et al.*, 2001]. Explicit lateral viscosity is null everywhere, except along sponge layers near open boundaries. Vertical mixing processes are parameterized with the nonlocal K-profile (KPP) boundary layer scheme [*Large et al.*, 1994] implemented for both surface and bottom boundary layers. The vertical diffusion terms are treated with a semi-implicit, Crank-Nicholson scheme to avoid time step restrictions due to large vertical mixing rates in the boundary layers and also in the interior when static stability needs to be restored.

[13] Our strategy for managing the large range of scales involved in this study is a multilevel approach based on the AGRIF package. This is an online (synchronous) nesting procedure which allows a rapid setup of a series of embedded domains with increasing resolution described by *Penven et al.* [2006]. The model grids, forcing, initial and boundary
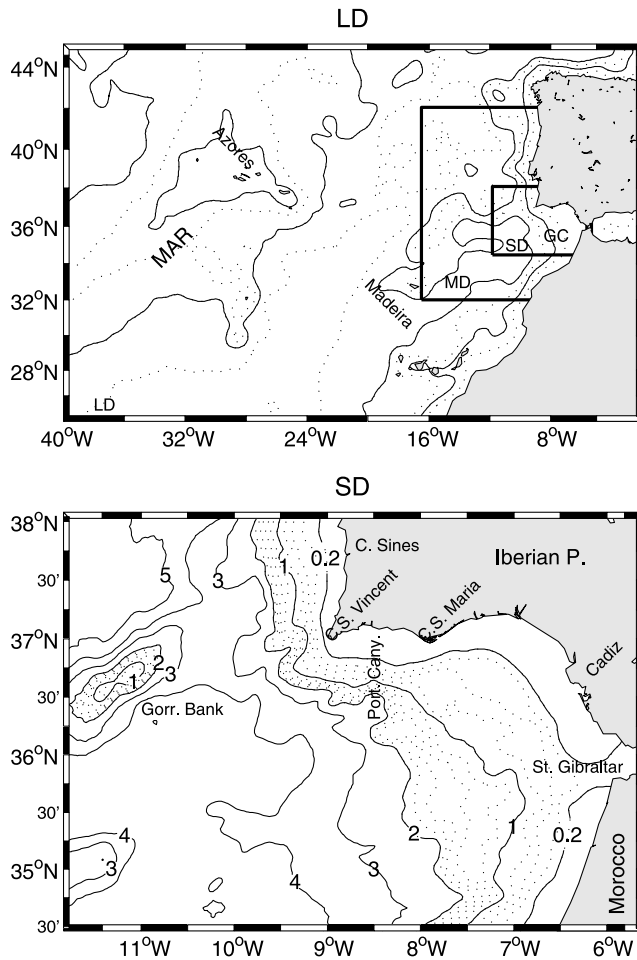
Figure 1. (top) Large-domain (LD) map including the midlatitude northeast Atlantic. Boxes represent the medium (MD) and small (SD) domains used in the nested configuration. The model bathymetry is represented using 2000 and 4000 m with solid lines and 3000 and 500 with dashed lines. The Mid Atlantic Ridge (MAR) crosses the domain in a southwest-northeast direction along the left half of the domain. (bottom) Gulf of Cadiz domain (SD) map. The model bathymetry is represented using 0.2 1- to 5-km isobaths (solid lines). Between 0.2 and 2 km the isobaths are represented each 0.2 km (dashed lines).

conditions are built using the ROMSTOOLS package [*Penven*, 2003].

3. Configuration Details

3.1. Large-Domain Experiment

[14] The ocean model experiments are conducted using 3 domains as shown in Figure 1. The large-scale domain (LD) is run independently and the intention is to provide initial and boundary conditions to the other domains, through a first stage of offline nesting. Resolution of LD is $1/8°$ ($\sim$10 km) in the horizontal which is below half of the Rossby radius near the Azores Current. The objective of the large grid is a good representation of the Azores Current transport and the Azores Current near Madeira where the western boundary of the higher-resolution grids is located.

30 sigma levels are used in the vertical and a stretching factor of $\theta_s = 0.6$; $\theta_b = 0$ [*Haidvogel and Beckmann*, 1999] to conserve a good near-surface resolution over the entire domain. The model bathymetry is based on National Geophysical Data Centre ETOPO2 2 minute topography [*Smith and Sandwell*, 1997]. The topography data (h) is interpolated into model grids and smoothed several times until the factor $r = \Delta h/2h$ [*Haidvogel and Beckmann*, 1999] is below 0.2. The part of the LD domain that includes the Mediterranean Sea is masked east of the longitude of the Strait of Gibraltar. The Western boundary is placed to the west of the Mid Atlantic Ridge (see Figure 1).

[15] The model is initialized from rest using January temperature and salinity climatologies from *Levitus and Boyer* [1994] and *Levitus et al.* [1994]. These same monthly climatologies are used to recycle temperature and salinity along the nudging bands and to provide open boundary data. Monthly surface fluxes are derived from Comprehensive Ocean-Atmosphere Data Set (COADS; referenced by *da Silva et al.* [1994]). Monthly geostrophic (referenced to 1200 m) and Ekman velocities are calculated from climatology and applied along open boundaries.

[16] Since the Mediterranean Undercurrent is not explicitly represented, a nudging zone is imposed in the interior to restore the temperature and salinity characteristics of the Mediterranean Water levels off the Gulf of Cadiz. This restoring element is based on a timescale that varies spatially according to $\mu(x, y, z) = 0.5\ (1/40)(\cos(\pi\ dr(x, y)/300.) + 1)\ (-\arctan(z + 750)\ 0.25/\pi + 0.5)$, where $dr(x, y)$ represents the distance in kilometers from $-9.5°$W $36.5°$N. This coefficient decays to zero within a radius of about 200 km and for depths above 700 m.

[17] Open boundary conditions were used for the southern, western and northern boundaries using Orlansky conditions for 3D momentum, Flather for 2D momentum and Upwind for temperature and salinity. Passive active conditions of *Marchesiello et al.* [2001], with inflow (outflow) nudging timescales of 1 (360) days for tracers and 10 (360) days for momentum respectively. Sponges were applied along the boundaries within a band of 6 grid cells. The viscosity coefficient A_h rises from zero in the inner part of the sponge to a maximum value of 1000.0 m^2/s. Out of the boundaries viscosity and diffusivity is zero. A linear drag formulation with a coefficient of 3×10^{-4} m/s is applied at the bottom.

[18] Similar methods to obtain equilibrium conditions were used for the California Current System by *Marchesiello et al.* [2003] and for the Peru-Chile system by *Penven et al.* [2005]. A spin-up experiment of 8 years was performed and equilibrium solutions are reached after the first 4 years (Figure 2). The model results presented below correspond to model years 4 to 6.

3.2. Nested Experiments

[19] The basin-scale experiments (LD) are also used to provide initial and boundary conditions for the mesoscale nested configurations. These configurations are constituted by two nested grids with a refinement coefficient of 3 (in time and space). The medium grid (MD; see Figure 1) covers the entire region around the Gulf of Cadiz and is limited in the west by the longitude of Madeira Island ($\sim$17°W). The cell size in MD is $1/11°$ ($\sim$7.5 km) in a
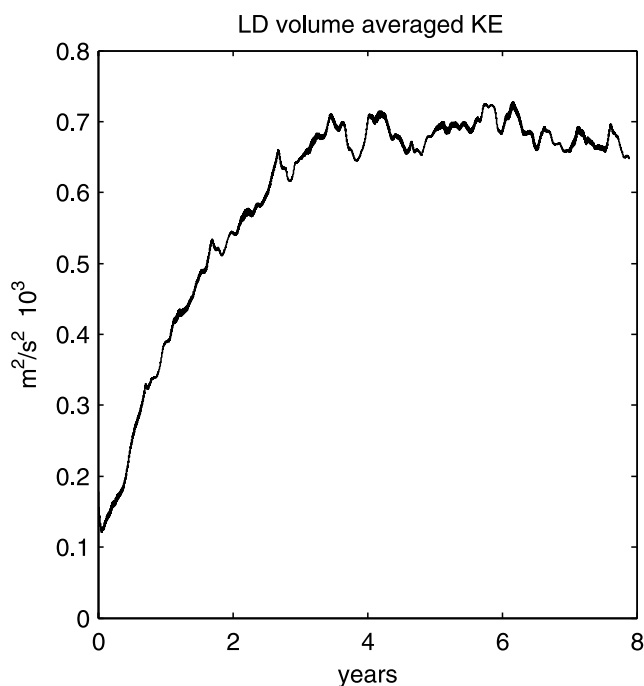
Figure 2. Time evolution of the volume-averaged kinetic energy for the large-domain experiment.

total of 124 × 140 grid points. The embedded grid covers the Gulf of Cadiz and Southwest Iberia zone (see Figure 1). The small grid (SD) is 206 × 149 with a resolution of about 2.6 km. A particular requirement for the representation of the Mediterranean Undercurrent is the good near-bottom resolution [*Serra et al.*, 2005]. A lower stretching factor is used θ_s = 0.4 and the number of vertical sigma levels is increased to 60. Topography data and smoothing strategy is the same as described for LD. Figure 3 shows a comparison between model SD grid topography and ETOPO2 original data. Given the high resolution of the grid, the topographic smoothing is very low and the grid bathymetry matches the data everywhere, with the exception of the slope zone between capes St. Maria and St. Vincent where model and original isobaths show a small lag.

[20] In the case of the MD, a two-grid-cell-wide channel of constant depth (300 m) is used to simulate the Gibraltar Strait (see map in Figure 4). The topography in SD is better resolved than in MD, which leads to discontinuities at the grids interface. To reduce these discontinuities, SD topography is forced to converge toward MD topography within a band of 10 grid points (25 km from the boundary). The initialization and boundary conditions are obtained using year 4 LD data which are stored as 10-day averages. These data were interpolated into the MD and the SD grids for the initial conditions, and into the MD grid for the boundary conditions. SD boundary conditions are obtained from MD by one-way online nesting. Control runs using year 6 LD outputs were also conducted.

[21] The exchange with the Mediterranean basin is represented explicitly by a fixed boundary condition imposed at the eastern edge of MD, which is landlocked everywhere except at the Gibraltar Strait. The inflow/outflow vertical setting shown in Figure 4 is based on the estimates of

Tsimplis and Bryden [2000] and *Baschek et al.* [2001]. The condition configures a two-layer system to match a transport of 0.8 Sv entering the Mediterranean Sea and 0.7 Sv exiting in the sublayer. The salinity and temperature of the outflow (Mediterranean flux into the model) are fixed at the following values: [bottom−250 m], 38.4/12.8°C; [250−200 m], 38.0/13.15°C; and [200−170], 37.8/13.2°C. All other values up to the surface vary according to the results of LD runs. A few tens of kilometers out of the Strait, the Mediterranean outflow accelerates and strong mixing processes occur [*Baringer and Price*, 1997a]. To simulate these subgrid-scale mixing effects a spot of increased horizontal mixing is imposed just off the Strait. Horizontal viscosity and diffusivity coefficients are calculated according to $A_h(x, y) =$ 500 $\mu(x, y)$[cm^2/s^2] where $\mu(x, y) = 0.5(\cos(\pi\, dr/70.0) + 1)$ and dr stands for the distance from the point of maximum mixing (isolines of μ are represented in Figure 4). Elsewhere $A_h(x, y) = 0$. However, strong gradients are eventually generated along the Mediterranean Undercurrent with the side effect of overshoot in the salinity fields. To avoid this problem a Smagorinsky viscosity condition was applied to the momentum equation. Finally, the spreading of the Mediterranean Water downslope is strongly sensitive to the bottom drag parameterization [*Serra et al.*, 2005]. For the nested configurations a quadratic drag coefficient of 5 × 10^{-3} is used.

[22] The experiments were conducted for 2 periods of 5 model months: the winter period from October to February and summer period from April to August. The data used in the analysis correspond to the last 2 months of each of these periods. This restriction is due to the explicit introduction of the MU, requiring an adjustment period of about 2 months for the establishment of the Meddy field (a realistic MU forms rather quickly).

4. Azores Current in the Large-Scale Solution

4.1. Mean Flow and Transport Variability

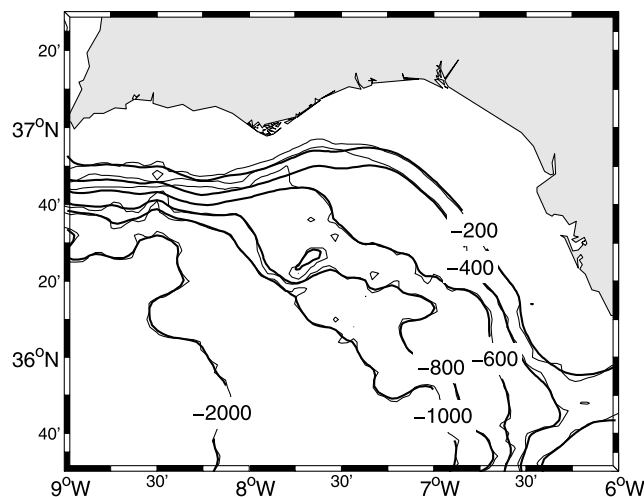[23] Figure 5 shows the stream function calculated using the time averaged outputs for model years 4−6 and inte-

Figure 3. Comparison of model SD grid topography (thick line) with Etopo2 [*Smith and Sandwell*, 1997] topography data (thin line) in the Gulf of Cadiz.
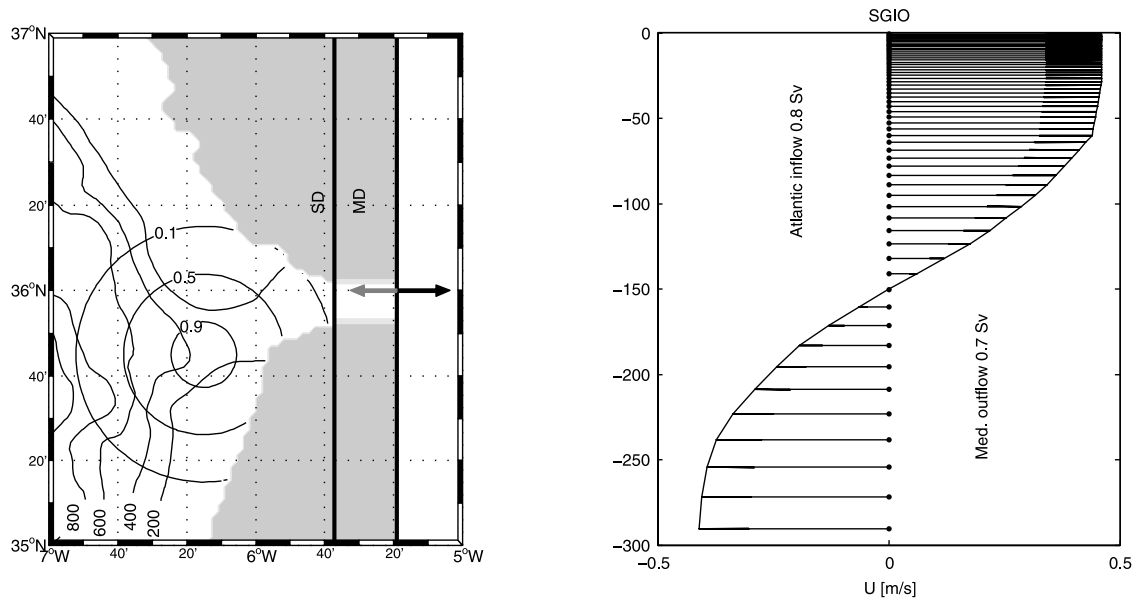
Figure 4. Scheme of the Strait of Gibraltar inflow outflow condition. (left) Point of application of the outflow (grey arrow into the domain) and inflow (black arrow out of the domain) in the eastern boundary of the medium domain (MD). The bathymetry along this part of the MD is idealized to be constant and equal to 300 m. The isobaths are plotted every 200 m. The circumferences show the spatial variation of μ the mixing coefficient applied in the SD (section 3.2). (right) Vertical distribution of the U velocity applied at the boundary point for each sigma level. The Strait of Gibraltar in MD is a two-cell-wide channel and the velocities are calculated to ensure an outflow of 0.7 Sv and inflow of 0.8 Sv (into the Mediterranean Sea).

grated in the upper 1000 m (see *Penven et al.* [2005] for the method of stream function computation). The lighter shades indicate anticyclonic circulation and the darker shade, cyclonic. The direction of the flow is such as the lighter shade is on its right.

[24] The AzC is located between 32°N and 36°N, and constitutes a dramatic change in the dominant meridional alignment of the circulation. The whole system, with the currents and countercurrents, spans a latitudinal band from 30°N to 38°N, where the net zonal flow is rather weak since the AzC is bordered by counterflows on both sides. The
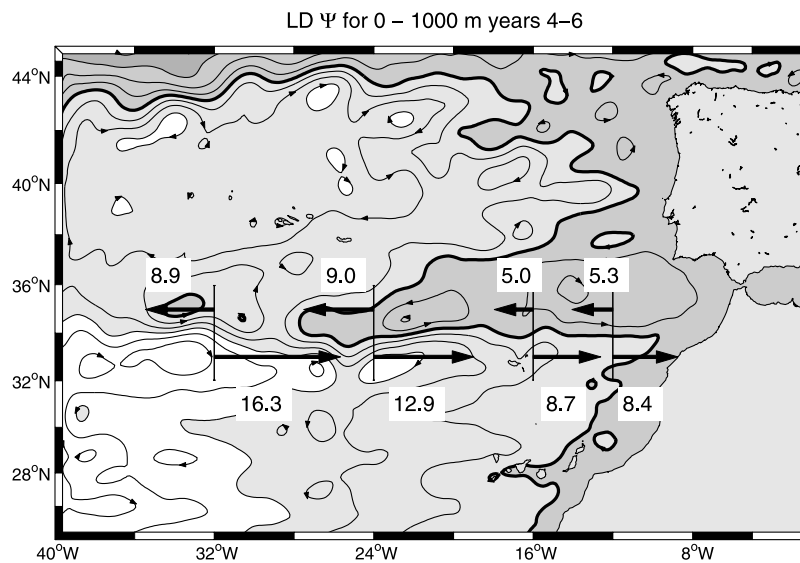

Figure 5. Stream function calculated using the nondivergent component of the time-averaged (years 4–6) and vertically integrated (0–1000 m) velocity fields. Lighter shades correspond to anticyclonic circulation and darker shades to cyclonic. Transport calculations using the same averaging intervals between 30°N and 38°N are represented for three given sections.
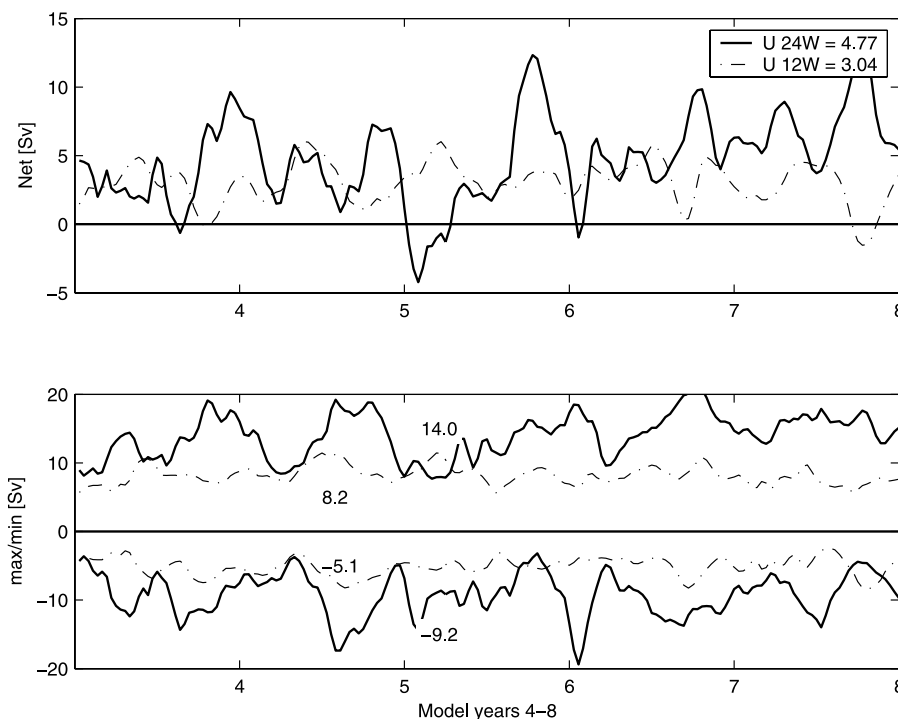
Figure 6. Near-instantaneous (10-day averaged) zonal transport time series calculated for the 24°W (solid line) and 12°W (dotted line) sections for the 0- to 1000-m layer (Figure 5). (top) Net transport for each section. (bottom) Eastward and westward components shown separately. The time series correspond to model years 4–8.

zonal mean circulation is weak everywhere out of the Azores Current region except in the northern part of the domain which is under the influence of the North Atlantic Current (north of 43°N). Figure 5 also shows time-averaged and depth-integrated east and west transports for several sections between 32°N and 36°N. The eastward flow is maximum in the western part (about 16 Sv) decreasing to about 8 Sv in the east. Part of the flow is deflected southward at a considerably constant rate between the western limit of the domain and the African coast. Another part recirculates westward with a maximum of 9 Sv south of Azores. The Azores Current expression in the stream function constitutes a steady zonal perturbation to the otherwise basin-scale smooth meridional flow. East of Madeira, a clear large cyclonic cell centered at 36°N and 16°W is observed off the Gulf of Cadiz. The net zonal flow for the 16°W and 12°W is very small (nearly zero if the meridional extension of integration increases) indicating an almost closed recirculation in this zone. There is a change in the mean flow structure about the Madeira Island longitude: West of Madeira, the mean zonal flow is dominated by the anticyclonic gyre recirculation, whereas to the east it is driven by the cyclonic recirculation cell off the Gulf of Cadiz.

[25] The transport values based on the time averaged flow are small if compared to the nearly instantaneous estimates based on the 10-day averaged outputs. Figure 6 shows the transport of the AzC (eastward) and counterflows (westward) time evolution for the last 4 years of the model simulation calculated in two sections at 24°W and 12°W. West of Madeira, the eastward transport oscillates around

15 Sv, with peaks sometimes exceeding 20 Sv, and being almost always above 10 Sv. These transport values are being compensated both north and south of the AzC by westward flow. The net transport is on average below 5 Sv, but significantly variable (see Figure 6, top). East of Madeira (12°W), the values for the east and west transports oscillate around 8 Sv and the net flow is substantially smaller averaging 3 Sv.

[26] No clear seasonal fluctuations of transport are evident but a nearly annual signal is apparent in the time series transport of the 24°W section (confirmed with spectral calculations; not shown). For the eastern section (12°W), subannual signals dominate. The considerable interannual variability in transport is interesting given the fact that the model is forced with the same forcing and boundary data every year. This leads us to conclude that the internal variability is an important factor for the local circulation (note for example the year 6 reversal in the net transport for 24°W section).

4.2. Comparison With Observations

[27] A comparison of averaged (model years 4–6) zonal velocities with a climatology produced with observations is provided in Figure 7 (bottom). The climatology produced with the Surface Velocity Programme (SVP) drifting buoys [*Lumpkin and Garzoli*, 2005] is smooth and, unfortunately, a very low number of observations exist in the vicinities of the Gulf of Cadiz. A good match is apparent between the model solution and the Azores Current climatology over nearly its whole zonal extent. The decrease in zonal flow at the longitude of Madeira referred to before, is observable in
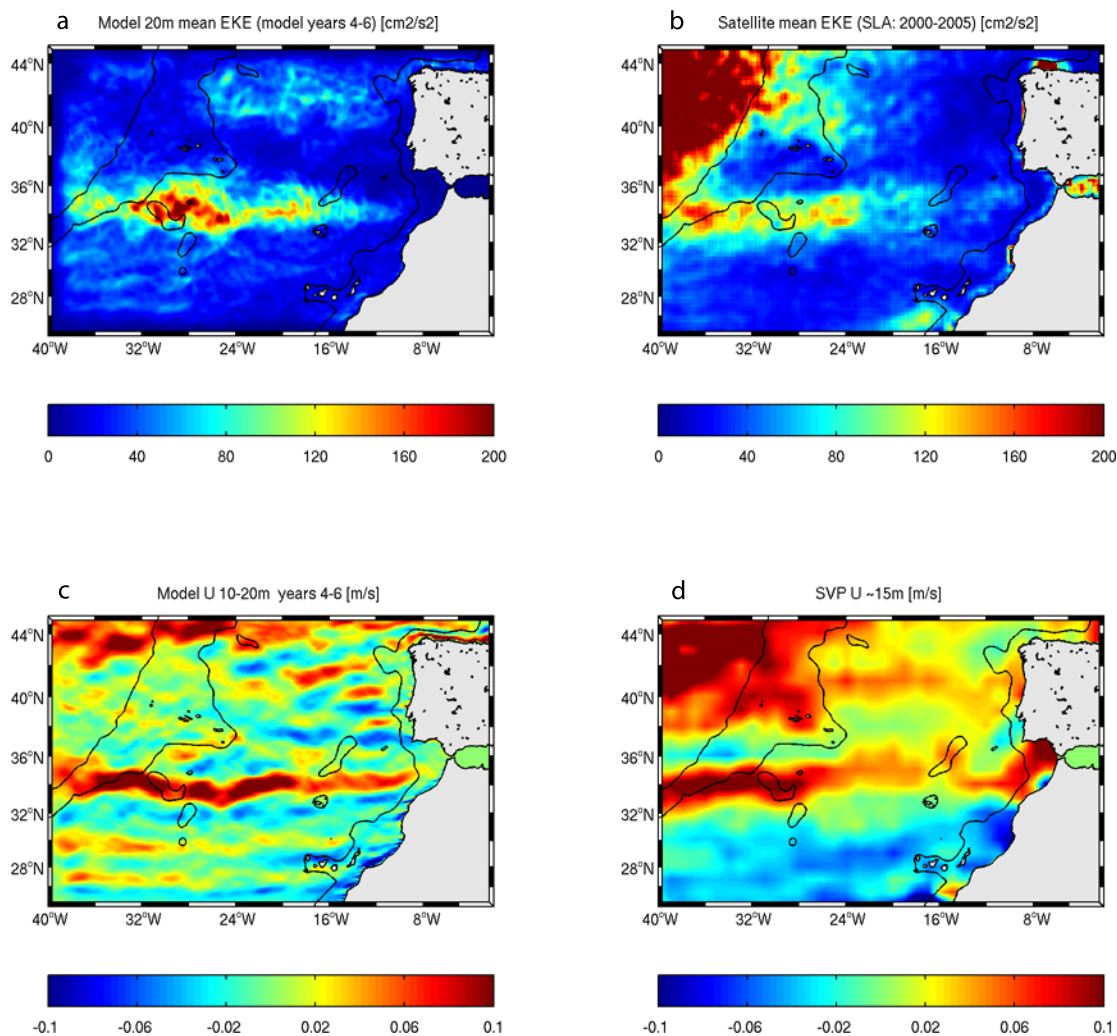
Figure 7.   (a) LD 20-m EKE average for the period 4−6 model years. (b) EKE from merged satellite altimetry surface level anomalies (AVISO program) for years 2000−2005. (c) Mean U velocities (model years 4−6) for surface layer 10−20 m. (d) Climatology from the Surface Velocity Programme (surface drifting buoys drogued at 15 m).

both the model and climatology. However, the model velocities between Azores and Madeira are higher than in the SVP climatology and the current axis is located more to the south. Considerable differences are also apparent west of the Mid Atlantic Ridge, since the model's western boundary value is climatological and underrepresents the inflow associated with the North Atlantic Current. Nevertheless, the eastward velocities at the latitude of the Azores Current on the west side of the domain are not very different from those in the climatology field. This indicates that a precise representation of inflow at the western boundary is not critical to the formation of the Azores Current inside the computational domain.

[28]   The underestimation of the flow west of the Mid Atlantic Ridge is also clear in the maps of mean eddy kinetic energy (EKE). Comparison between model and altimetry-derived EKE is represented in Figure 7 (top). The model largely underestimates the EKE west of MAR in the northern part of the domain, owing to marginal representation of the North Atlantic Current variability. However, the comparison shows a good match along the axis of the Azores Current. Along 34°N, the magnitude and zonal structure of model EKE are similar to the SLA-derived EKE climatology. The comparison is poor again near the Gulf of Cadiz, characterized by smaller eddies which may be subsampled by the satellite.

[29]   The model mean vertical current structure is shown in Figure 8 at 20°W and 14°W for comparison with two existing WOCE sections. In the west section, the core of the mean AzC is around 34°N and about 2 degrees wide. It shows broader counterflows on north and south sides. The velocity values are significant down to depths of 1000 m with maximum on the order of 0.14 m s^{-1} at the surface. The counterflow is less intense but broader and deeper and equally surface intensified. The westward undercurrent described by *Alves and Colin de Verdière* [1999] is not a sharp feature in the sections, but evidence of it is seen on the west side of the domain (not shown). The mean vertical flow structure at 14°W shows less intensified flows and counter flows. The core of the AzC is still at about 34°N but a less clear meridional organization is observed (note that the topography is complex along this section).
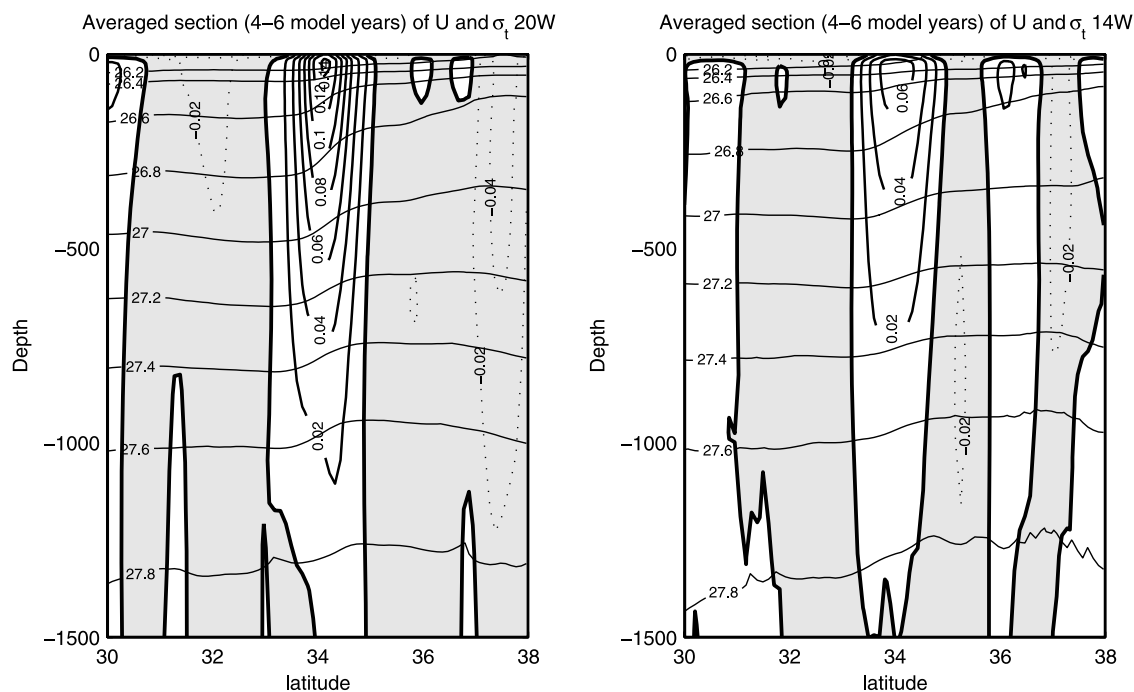
Averaged section (4–6 model years) of U and σ_t 20W   Averaged section (4–6 model years) of U and σ_t 14W

Figure 8. Averaged sections of u and σ_t at $-20°W$ and $-14°W$. Zones of negative (westward) values are shaded and lines are plotted each 0.02 m s^{-1} (dotted and solid lines indicate, respectively, westward and eastward currents). The σ_t lines are plotted each 0.2 kg m^{-3}.

[30] Given that data on zonal transport in the eastern part of the Azores Current are rare, two WOCE meridional sections surveyed in two different years are presented in Figure 9. The geostrophic velocities and the transport estimates are referenced to 1500 m. The arrows and values indicate westward and eastward transport estimates. The geostrophic velocities are higher than the model mean fields but of comparable magnitudes, and are within the range of the nearly instantaneous transport time series of Figure 6. The observed sections show various currents and counter

currents which are also discernable in the model mean section at 14°W.

[31] In summary, the model results provide an accurate representation of the Azores Current particularly in the vicinity of the Gulf of Cadiz where the higher-resolution nested experiments are conducted. The AzC is aligned at about 34°N with maximum transports in the west around 15 Sv but decaying to less than about 8 Sv east of Madeira. The flow is bounded to the north and to the south by broader and deeper (though less energetic) counterflows.
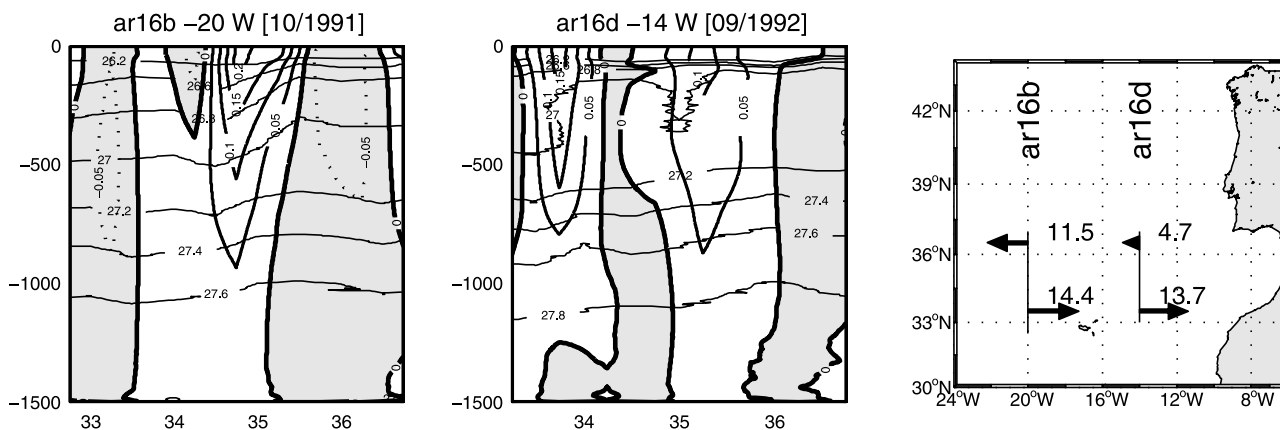
ar16b –20 W [10/1991]   ar16d –14 W [09/1992]

Figure 9. WOCE sections and corresponding transport estimates down to 1500 m (the reference level). The data are part of larger CTD surveys from the WOCE Eastern Boundary Current research (German contribution) conducted in September–October of two consecutive years 1991 (ar16b) and 1992 (ar16d). The depth of the stations is about 2000 m, and the sections cover a larger meridional zone (to the north) than is shown here. Shades and dotted lines correspond to westward current (lines are plotted each 0.05 m s^{-1}). The σ_t lines are plotted each 0.2 kg m^{-3}. The right-hand plot indicates estimates of total eastward and westward transports (down to 1500 m) in the sections in Sv.

Evidence of an undercurrent along the northern edge of the AzC is clearer in the western part of the domain. East of Madeira the flow seems to be associated with a large cyclonic recirculation cell as predicted by β-plume models. There is no clear seasonal signal but interannual and nearly annual fluctuations are present, though east of Madeira the subannual signals dominate. The simulation seems to reach a nearly steady state by year four, and since the model does not recover completely the characteristics of the intermediate Mediterranean Water, a decision was made to use year 4 to provide initial and boundary conditions for the nested base case experiments. To access the importance of the interannual variability, the nested configurations were also run based on year 6 LD outputs.

5. Mediterranean Undercurrent (MU) and Meddies

[32] Although the objective of the present study is the surface circulation, the Mediterranean Undercurrent and the Meddies are conspicuous, and very energetic circulations features that require adequate representation in a model of the Gulf of Cadiz. In particular, the interaction of the MU with the surface layer is a potential mechanism for driving a strong surface mean flow [*Jia*, 2000; *Özgökmen et al.*, 2001; *Kida*, 2006]. Concurrently, the Atlantic inflow into the Mediterranean is on the order of 1 Sv and is expected to have some impact on the surface circulation at least in the eastern part of the Gulf of Cadiz. In the nested experiments, the water exchange across the Strait of Gibraltar is explicitly represented through the boundary condition previously described. The spreading of the Mediterranean outflow and the generation of Mediterranean Undercurrent are very complex processes from the modeling point of view, since strong gradients are generated across small horizontal and vertical scales. In this context, the bottom boundary layer and mixing are critical for a good representation of the water properties, bottom flow advection and a buoyancy adjustment at correct depths [*Baringer and Price*, 1997a, 1997b; *Mauritzen et al.*, 2001].

[33] Despite the difficulties, the obtained MU is very similar to the one that has been reported in observational and in process-oriented or more simple modeling studies [*Serra et al.*, 2005; *Papadakis et al.*, 2003]. The plume thickness is between 50 and 100 m and it accelerates a few tens of kilometers off the Strait to maximum values on the order of 1.0 m/s. Strong mixing occurs right at this point inducing a significant drop in salinity maxima, although the model salinity is always above the usual registered values. The plume is bottom advected with a significant cross-isobath component and interacts with several topographical features splitting near to prominent bottom topography, one close to 36°N−7°W and the other south of Cape St. Maria (see Figure 1). Downstream of these locations, the slope gets steeper and the MU double core structure recurrently reported in literature [e.g., *Ambar and Howe*, 1979], is obvious in the velocity fields but is not evident in the salinity vertical field (Figure 10). This is perhaps associated with the model's incapacity to accurately represent all the details of the mixing processes. The lower core of the Mediterranean Water plume at the Cape St. Vincent longitude is between 1200 m and 1400 m. The velocity cores are however shallower; around 600 m (upper) and 1000 m (lower) with velocities of about 0.4 m/s.

[34] The plume detaches mainly off Cape St. Vincent with anticyclonic eddy generation but other Meddies generate after perturbation growth past Portimao Canyon. Figure 10 shows two dipoles rooted in the slope near Cape St. Vincent. The one to the south is generated after the meandering of the MU, whereas the one to the west results from the anticyclonic separation of the flow [*Bower et al.*, 1997]. The core of the Meddies varies between 700 and 1200 m with the velocity core placed upslope of the salinity maximum. They show velocities on the order of 0.2 m/s rarely exceeding 0.3 m/s, and core salinities from 36.2 to 36.6. Model Meddies show significant velocity up to the surface, in some cases as much as 0.1 m/s. Meddy vorticity values are within the estimates not exceeding $0.3 - 0.4\ f$ [*Bower et al.*, 1997; *Serra and Ambar*, 2002; *Carton et al.*, 2002].

[35] During the simulation period, about 5 to 6 Meddies detach usually with cyclonic counterparts. This rate of eddy shedding compares well with the 17 per year estimate of *Bower et al.* [1997]. Strong interaction between recently generated and other Meddies occurs permanently providing pathways for offshore stirring of slope saltier water (salty filaments) as documented by *Carton et al.* [2002]. Some of the eddies evolve very fast and eventually dissipate or merge after eddy-eddy or eddy-topography interactions. A number of anticyclones last longer, and with time tend to acquire a circular isolated shape with space scales of about 50 km, for example, the Meddy in the cross section of Figure 10. The vertical structure of newly formed Meddies shows a slanted salinity anomaly wrapping around the eddy core and a heterogeneous eddy center is observed (this fact has never been reported in observational or in other modeling studies but it is beyond the scope of the present paper). With time the mixing processes produce a homogeneous eddy center.

[36] In summary, the main characteristics of the MU and Meddies reported in observations and in process oriented models are well represented in the nested experiments. In particular, the dynamical characteristics of the obtained MU and Meddies are very similar to the observed ones, for example, the Meddy field described by *Carton et al.* [2002]. Concerning water mass characteristics, the model fails to correctly reproduce all the details of mixing and entrainment, and the MU salinities are higher and sometimes the model MU is denser and deeper than is generally reported in observations. Notwithstanding, an event of denser and deeper MU similar to the present results is reported by *Serra and Ambar* [2002] and *Borenas et al.* [2002].

6. Mean Flow Structure in the Gulf of Cadiz
6.1. Cyclonic Recirculation in the Gulf of Cadiz

[37] Figure 11 shows the stream function calculated for the vertically integrated 0−600 m and time-averaged flow for winter and summer for the SD experiments. The time-averaging refers to the two last months of each 5-month simulation with explicit representation of Mediterranean Undercurrent initialized with year 4 (or year 6 where referred) outputs from LD. It should be noticed that although the stream function gives a useful representation of
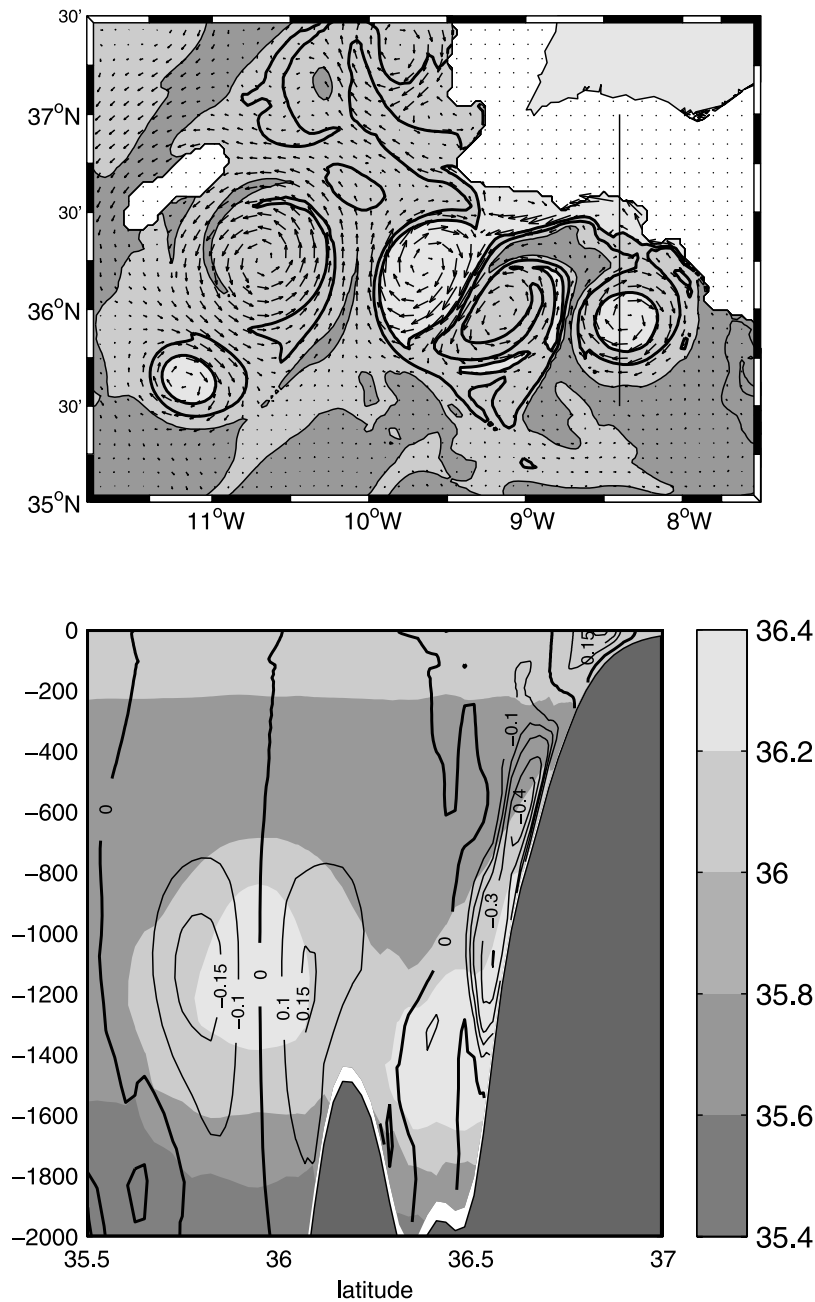
Figure 10. Example of instantaneous fields for month 4 of winter case. (top) Salinity and velocity vector field at 1000 m depth. Isolines correspond to 36.2 and 36.4 salinities. (bottom) Cross section (location represented in the top plot) of salinity (shades) and velocity (lines plotted each 0.1 m/s with the exception of 0.15 and −0.15, also shown).

flow structure, it includes only the nondivergent component of the flow and does not account for the expected and significant cross-isopycnal transport due to entrainment. To have a better and more precise insight into the transport analysis a second method is used. Instantaneous cross-section transports are calculated and then time-averaged. The transports and budget calculations are represented in Figure 11 (bottom).

[38] In both seasons, the flow enters the GoC from the southwest, circulates cyclonically and returns offshore in a west-northwest direction generating a large recirculation cell similar to that predicted by the topography and eddy-driven β plume of *Kida* [2006]. Part of the flow is associated with an anticyclonic recirculation to the south which is clearer in the summer case, Figure 11b. In both seasons, part of the flow reaches the Strait of Gibraltar zone and a small cyclonic recirculation is observed just off the strait. The larger cyclonic recirculation is constituted by one or more closed cyclonic cells. The secondary cells are the expression of persistent eddy activity in the intermediate layer. The top panel of Figure 10 shows the instantaneous situation by month 4 of the winter simulation. Some of the
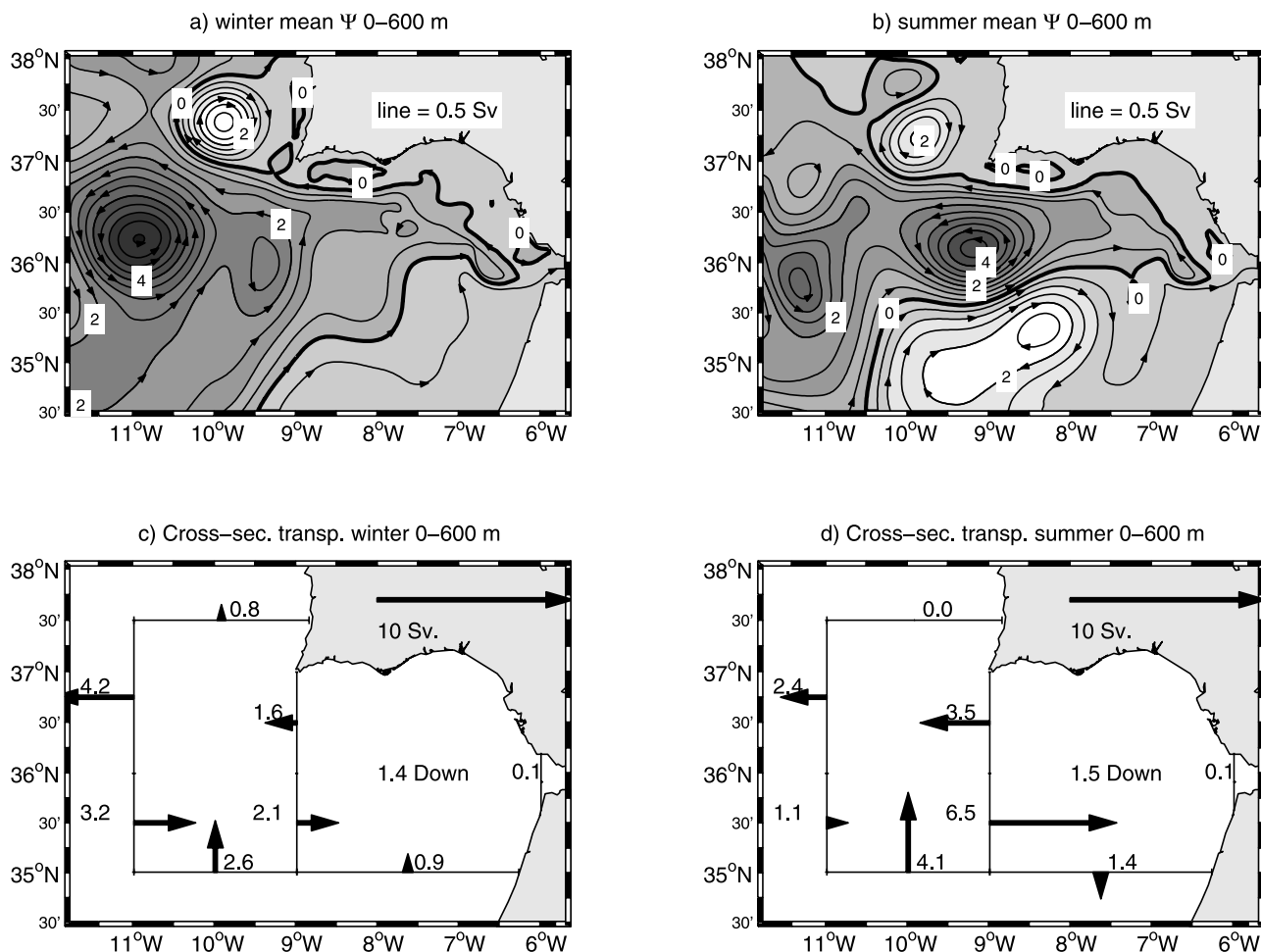
a) winter mean Ψ 0–600 m

b) summer mean Ψ 0–600 m

c) Cross–sec. transp. winter 0–600 m

d) Cross–sec. transp. summer 0–600 m

Figure 11. Stream lines for the upper 0- to 600-m layers for (a) winter and (b) summer plotted each 0.5 Sv. The stream function is calculated from the time-mean solution of month 4–5 (corresponding to July–August in summer and to January–February in winter) and vertically integrating the layer 0–600 m. Labels show the transport between thinner lines and the thick line. Darker shades correspond to cyclonic circulation. (c, d) Time-mean, cross-section transport values (Sv) in the 0- to 600-m layer.

eddies remain for long periods leaving a signature in the stream function of the mean flow.

[39] It is not possible to draw conclusions about the seasonality of the cyclonic recirculation from the present experiments. The apparent difference in flow intensity inside the Gulf of Cadiz between summer and winter is not confirmed when winter and summer situations based on year 6 LD outputs (not shown) are compared. It seems that these differences are associated with the turbulent evolution of the Meddy field and not with any external seasonal forcing.

[40] The budget for the eastern box (Figures 11c and 11d) shows that the vertical mass flux associated with the entrainment is on the order of 1.5 Sv. A value of nearly 4 Sv recirculates in or about the Gulf of Cadiz. Larger values can be observed but these are associated with localized recirculation cells (e.g., see summer case in Figures 11b and 11c). The circulation is mostly from the southwest to the west and the contributions from the northwest African coast are very small (∼1 Sv) though a seasonal change in orientation should be noticed.

[41] To filter out the effects of eddies in the stream function, a larger time-averaging was produced using the four experiments outputs (summer and winter of year 4 and of year 6). The results are reproduced in Figure 12. A clearer picture of the cyclonic recirculation cell can be observed that is much closer to the β-plume flow structures of Kida [2006]. A value of ∼3.5 Sv recirculates inside the Gulf of Cadiz in the surface 600 m. The cell expands from the southwest to the west but some recirculation inside the domain along the western boundary is observed. This recirculation may be partially associated with fact that the one-way nested boundaries are not absolutely transparent to flow structures generated inside the domain.

[42] To confirm the robustness of the results to the variations of external forcing, two additional experiments were produced. In the first experiment, initial and boundary conditions were modified to obtain horizontally homogeneous temperature and salinity fields with vertical variations derived from the profiles near 36°N and 10°W (Figure 13a). In a second experiment, (Figure 13b) the explicit representation of Mediterranean Undercurrent was shutoff and the nested simulation was used only for downscaling the large-
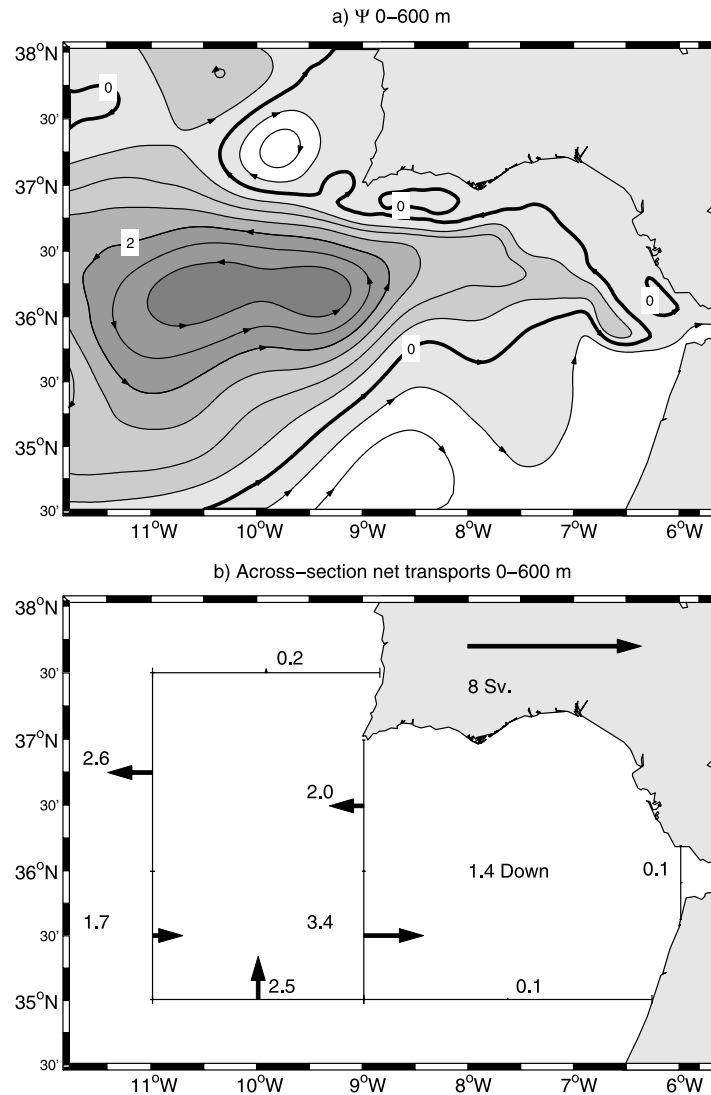
Figure 12. Stream lines for the upper 0- to 600-m layers using averages from January–February and July–August experiments forced by year 4 and year 6 of the large-scale model simulation. The plots represent the same as in Figure 11.

scale solution (summer of year 4). The comparison between the two stream function fields shows that although a weak recirculation is produced without the MU condition, the cyclonic cell is only simulated when the MU is introduced in the model. On the other hand, the flow field in the case with horizontally homogeneous initialization (no lateral momentum forcing (Figure 13a) is smooth and very similar to the solution given by extended averaging (Figure 12a).

[43] The role of the inflow of surface Atlantic water into the Mediterranean is assessed in another independent experiment. To that end, the Gibraltar exchange condition (Figure 4) was modified to retain only the Mediterranean outflow (no inflow experiment). The stream function calculated with the time-mean flow of this experiment is represented in Figures 14a and 14c. The stream function and transports do not differ significantly from the base experiment (Figures 11a and 11c). This result was expected since the cyclonic circulation is mostly controlled by the outflow. Additional experiments to evaluate the model

sensitivity to varying degrees of entrainment were also conducted. Various degrees of enhanced horizontal mixing near the strait $A_h(x, y)$, discussed in section 3.2, were tested (without varying the vertical mixing). Without any horizontal mixing at all ($A_h(x, y) = 0$), the changes are dramatic: the Undercurrent behavior becomes unrealistic with exaggerated descent rate as well as early separation and Meddy formation. Results for an intermediate case of mixing (coefficients reduced to a quarter of the basic case values) are more interesting (Figures 14b and 14d) since the MU reproduced by the model still shows an acceptable degree of realism. In this case, a significant reduction in downward transport (from 1.5 Sv to 1.0) is noticeable, and weaker circulation is produced confirming the role of entrainment on the generation of the β plume.

[44] To summarize, a time-mean recirculation cyclonic cell is formed from the Gulf of Cadiz westward with characteristics very close to the ones predicted by the β-plume models of *Kida* [2006]. A value of about 4 Sv
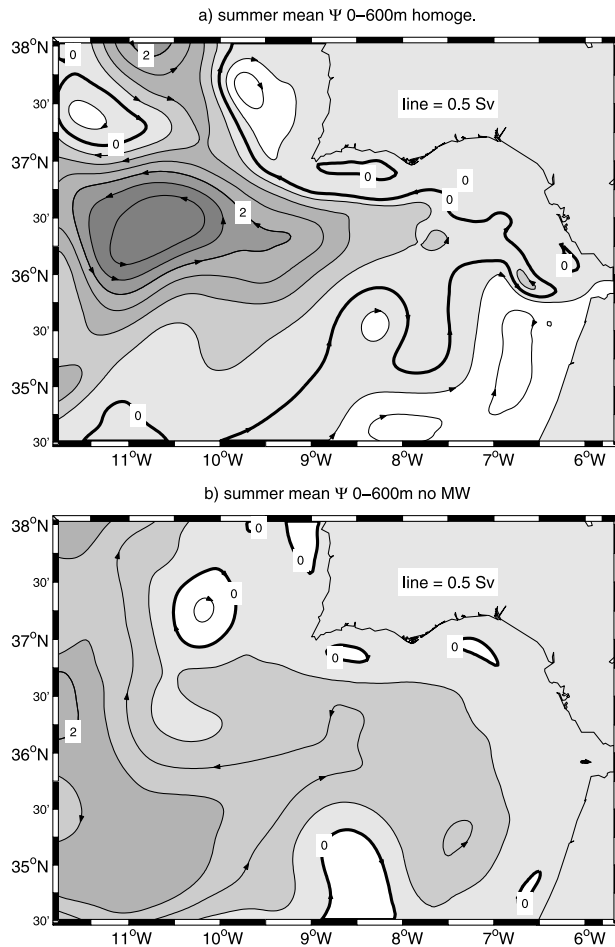
Figure 13. Stream lines for the upper 0- to 600-m layers (a) for horizontally homogenous case and (b) for the case with no MW.

recirculates in the surface 600 m (nearly 5 Sv if the integration goes down to 1000 m deep). The main features of the cyclonic cell develop very soon after 2 months (not shown) of MU activity but it is strongly masked by the eddy field. No clear seasonal changes are seen in the cyclonic cell that is generated (the β plume), since its main forcing factor is the MU, which in the model is seasonally invariant (also no significant seasonal changes have been reported in observations). Finally, the external forcing seems to exert little influence in the formation of the cell, confirming that the β plume is generated inside the Gulf and is driven by the MU.

6.2. Vertical Structure

[45] Figure 15 shows the vertical structure of the mean salinity (shades) and zonal current (lines) for winter (Figure 15, top) and summer (Figure 15, bottom). In the westernmost section at 8.8°W (Figures 15a and 15c, left), the MU reaches a buoyancy equilibrium and spreads laterally. The salt tongue spreads offshore at the proper depths although the separation between the upper and lower cores reported in some of the observational works is not perceptible. On the other hand, the velocity jet of the MU spans from nearly 400 m to the 1400 m depth. Two clear cores of around 0.3 m/s of mean current are observed at 600 m and

below 1000 m depth. The westward slope current reaches the surface but with values below 0.05–0.1 m/s. Off the slope, the flow is broad and deep and is oriented eastward. The summer case (Figure 15, bottom) shows a sharp zonal flow that is associated with the intensified recirculation cells referred to above. In the winter case (Figure 15, top), the eastward current is weaker but broader.

[46] To the east, in the section at 7.5°W (Figures 15b and 15d), the MU is still progressing down slope. The coupling between the eastward flow and the Mediterranean Undercurrent is clearly perceptible. As the MU flows west and downslope, with mean flow maximum around 0.35 m/s, it induces a stretching of the upper layer. The whole upper column responds barotropically and flows eastward. Within about 200 m above the MU (see velocity structure in Figures 15b and 15d at about 36.25°N), this flow accelerates in equilibrium with the strong lateral density gradient, reaching maximum velocities of about 0.15 m/s. At this longitude the MU counterflow is observable around 700 m depth (see Figures 15b and 15d). This core is observed at shallower (deeper) depths eastward (westward) since the MU is also shallower (deeper) in the eastern (western) part of the Gulf. The coupling between the faster downslope Mediterranean Undercurrent and the slower barotropic flow (intensified near the MU core), is observable all the way along the downslope path of the MU. The barotropic flow vanishes where the MU reaches buoyancy equilibrium with offshore background.

[47] In the shallower part of the slope, a secondary current system is observable. Near the bottom, the second MU core around 500 m is much weaker in places reaching 0.2 m/s, and the coupling with the surface counterpart is not clear. The upper eastward flow is around 0.15 m/s in its surface core and it separates from the slope in the summer case. Note that elsewhere, the flow structure in the 7.5°W section is very similar between the winter and summer experiments. This surface, along slope, eastward flow averages around 0.4 Sv and is also observable in the western section (Figures 15a and 15c). It is a very persistent and continuous flow feature all the way along the northern slope of the Gulf of Cadiz which we will term the Gulf of Cadiz slope Current (GCC).

[48] Figure 16 shows the horizontal current vectors for given depths in winter and summer. In the surface case (at 20 m; top row), we can observe the GCC all along the slope from the Cape of St. Vincent to the Strait of Gibraltar. In the summer experiment, the GCC is connected upstream with the upwelling current of the southwestern Iberian slope. In the winter case (Figure 16a), the continuity is not clear since the flow seems to be dominated by the anticyclonic recirculation and by the offshore separation recurrent off Cape. S. Vincent. However, for part of the time, the flow is also continuous with the southwest coast circulation. Southeast of Cape St. Maria the flow seems to separate offshore in the summer experiment, in a way that is consistent with observations of a clear surface thermal signature usually referred to as the "Huelva Front" [e.g., *Relvas and Barton*, 2002; *Garcia-Lafuente et al.*, 2006]. East of Cape St. Maria, the GCC seems to split between slope and shelf currents. The winter mean flow is strongly affected by the transient eddy activity since the alongshore winds are weak. In summer, the southwest wind component is important and
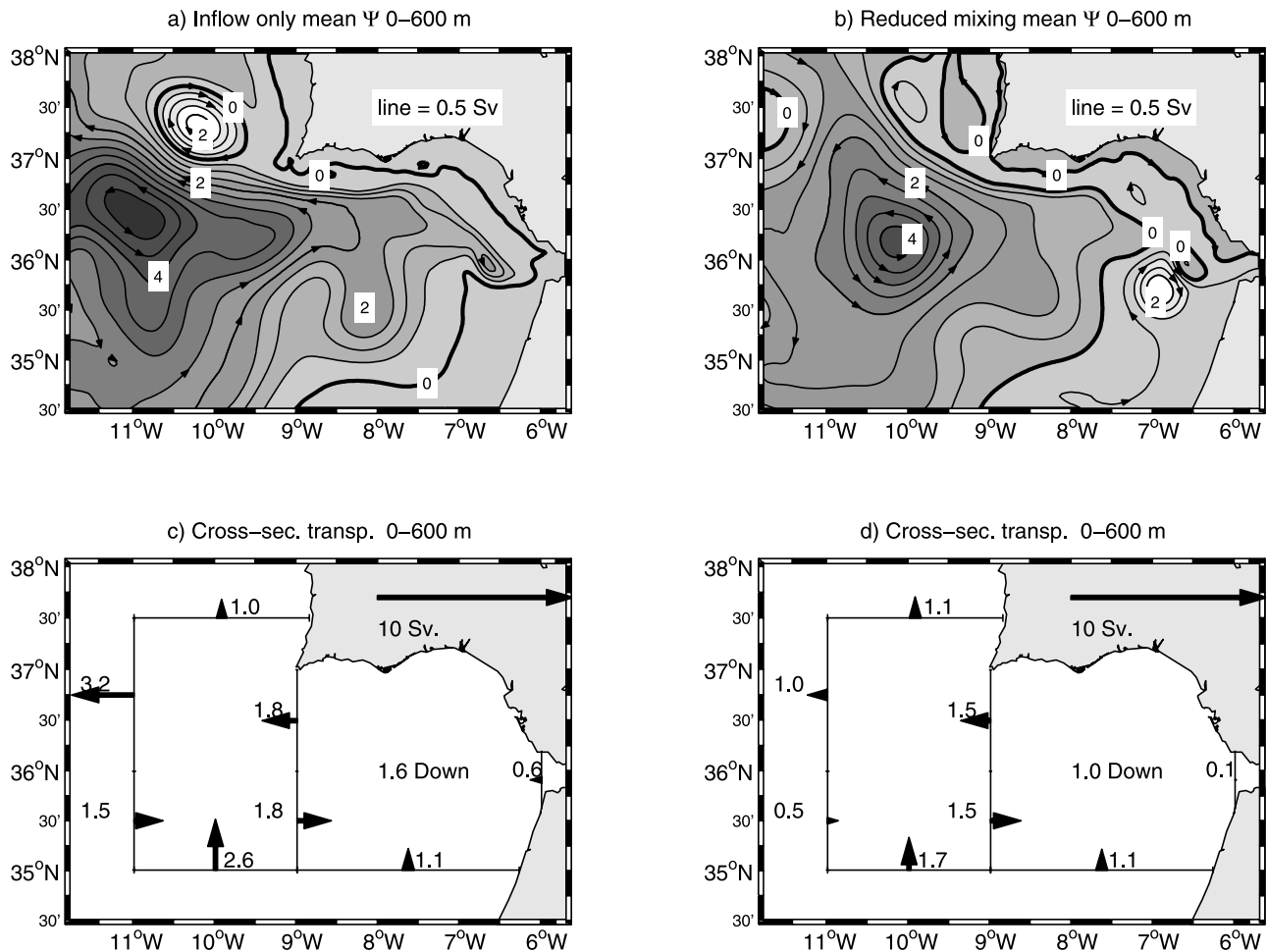
Figure 14. Same as in Figure 11 for two sensitivity experiments: (a, c) experiment with no inflow from the Atlantic into the Mediterranean; (b, d) experiment with reduced mixing coefficients (one fourth of central experiment) to simulate low entrainment conditions.

the bulk of the current is observed over the shelf, whereas over the slope, the flow is weak and intermittent owing to the separation past Cape St. Maria. The fate of the GCC is the inflow into the Mediterranean Sea. Near the Strait, the GCC merges with a stronger flow (the Mediterranean Undercurrent counterflow) to feed the Atlantic inflow.

[49] The small cyclonic cell located just off the strait is the expression of a strong convergence associated with intense entrainment occurring mainly in that point. The flow converges from the south and from the west in about equal contributions. Part of the flow subducts and another part joins the GCC into the Mediterranean. At the 200 m level (Figures 16a and 16c), the flow direction at the Strait of Gibraltar is entirely out of the Mediterranean and the GCC is no longer noticeable. However, there is still a strong convergence into the mouth of the Strait from the west, associated with the MU counterflow, and with a small contribution from the south. At 400 m (Figures 16a and 16c), the MU is already the clearest feature along the slope. The flow into the entrainment zone is now only from the west. Also, the entrainment zone and its associated cyclonic recirculation is displaced northwestward along the slope. A strong cyclonic current bordering the MU in the opposite

direction (the MU counterflow) is always present. The zone of convergence and cyclonic recirculation is observed farther west in the 600-m field. At this depth, the recirculation is already north of 36°N and west of 7°W (compare with 20-m and 200-m levels). The cyclonic flow running opposite to the MU is now near 7.5°W hence observable in the vertical sections (Figures 15b and 15d). It corresponds to the current located on top of the MU offshore edge that has been previously discussed.

[50] A further confirmation of the link between the GCC and the inflow is shown in Figure 17. The two plots compare the winter mean velocity at 20 m depth for the base experiment (Figure 17a), and for the experiment with no inflow from the Atlantic into the Mediterranean (Figure 17b). It is clear that in the no inflow experiment, the Gulf of Cadiz slope Current disappears leaving space for the MU to surface in the western part of the slope (~9°W).

[51] To briefly recapitulate, the Mediterranean outflow in the present model induces a strong entrainment and upper layer steering that controls the eastern part of the Gulf of Cadiz. The bulk of the entrainment occurs along the offshore edge of the MU, and while it progresses downslope the upper layer is forced to respond with a counterflow by
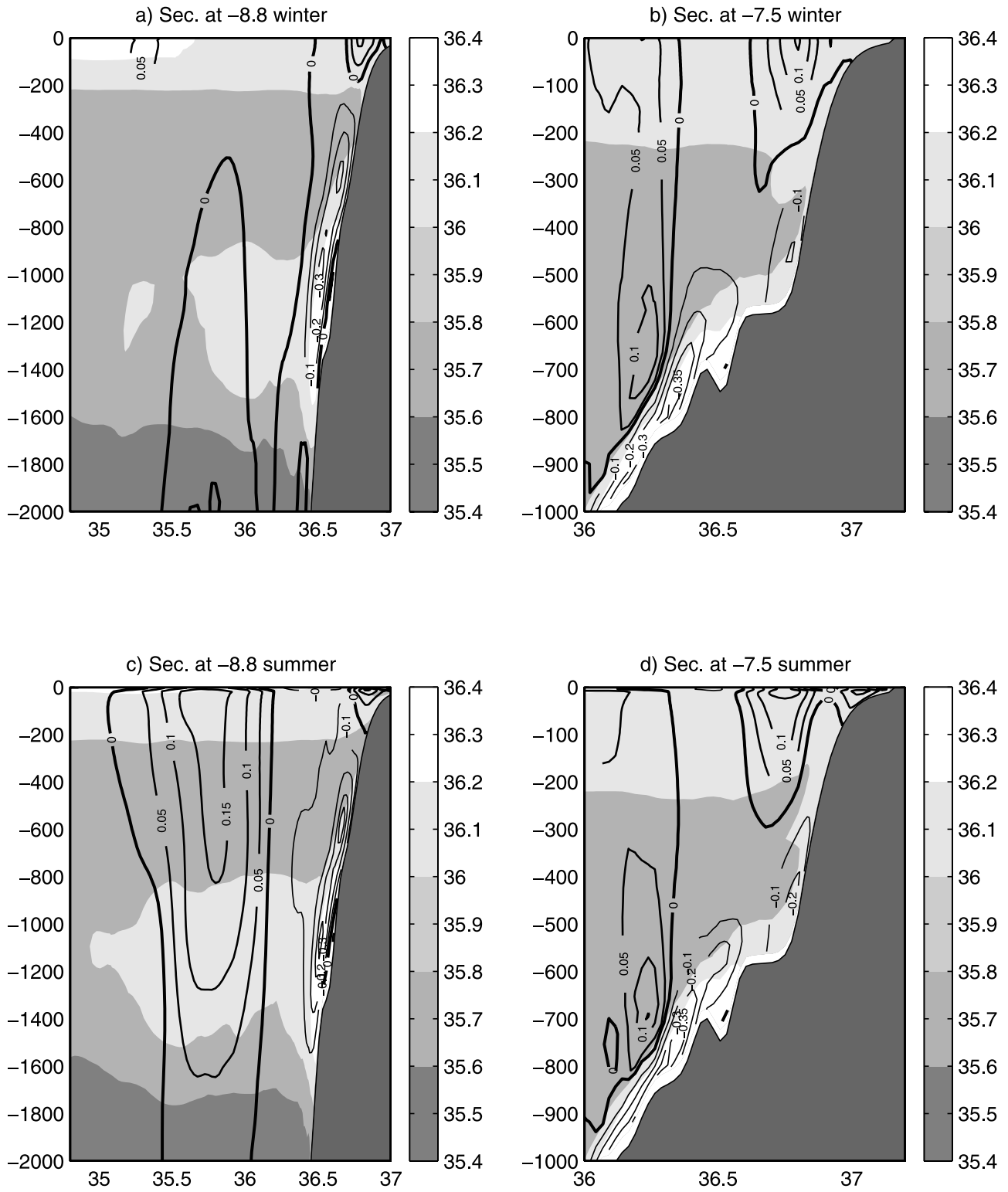
Figure 15. Vertical structure of the time-mean flow for (top) winter and (bottom) summer along two sections on the (left) west and (right) east of the Gulf of Cadiz. The shades represent mean salinity. Lines show the zonal velocity component. Thick lines mark the eastward flow (lines are plotted each 0.05 m/s).
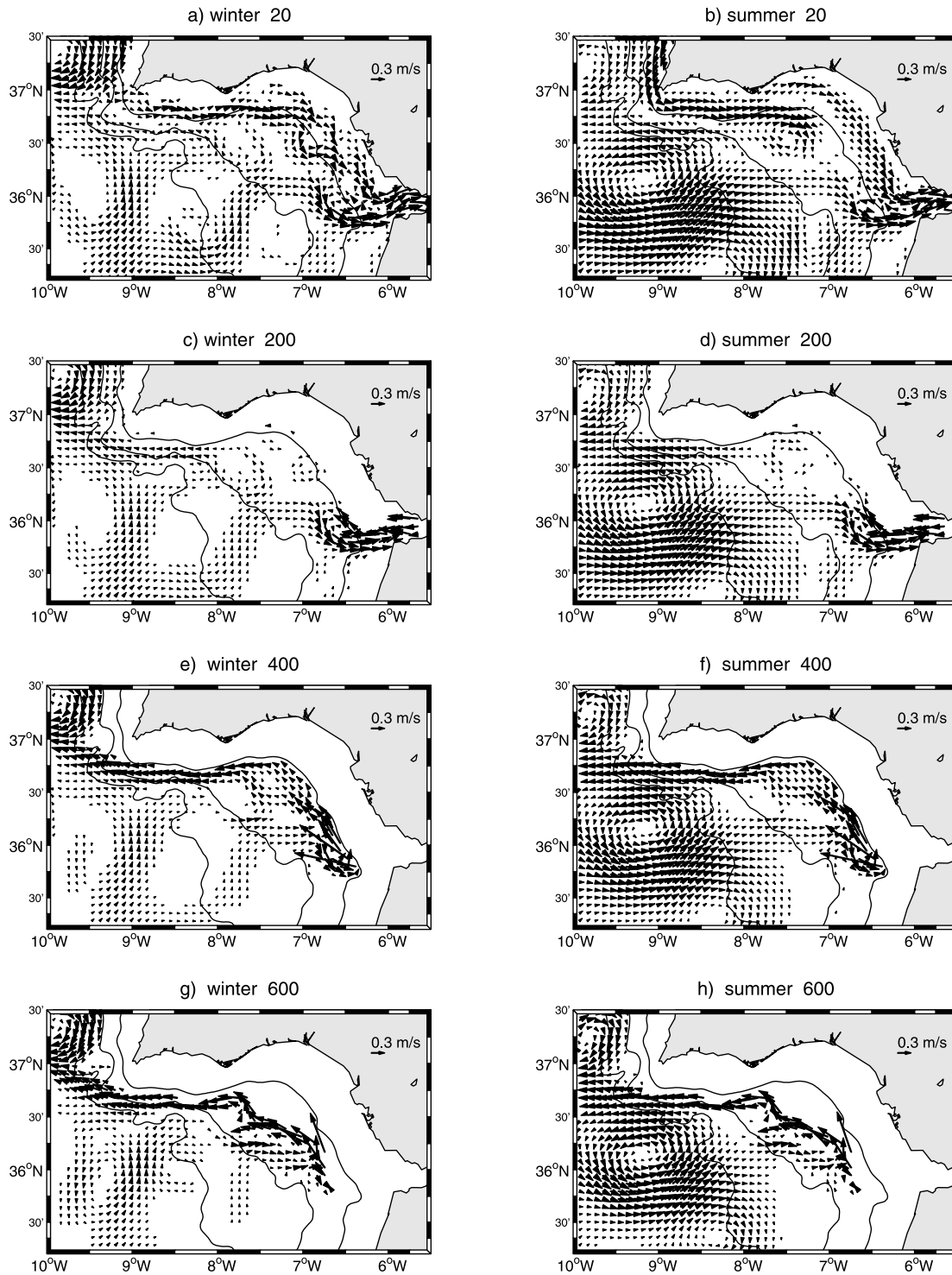
Figure 16. Time-mean flow vectors at different depth levels (20, 200, 400, and 600 m), for (left) the winter averaged period and (right) for the summer averaged period. The 400-, 1000-, and 2000-m isobaths are represented.

thermal wind. The current running in the opposite direction is intensified on top of the offshore side of the MU, where the sharper density gradients are produced. Part of this counterflow is entrained by the MU and another part of it recirculates horizontally along the slope westward (i.e., alongside and on top of the MU). At shallower levels, this

recirculation happens very near the Strait and slowly deepens and changes westward with the MU. In this process, a broad flow is captured into the slope to generate a narrow westward slope jet intensified at intermediate depths. Above the 200 m, a small part of this flow enters the Mediterranean. However, since this is not sufficient to make the
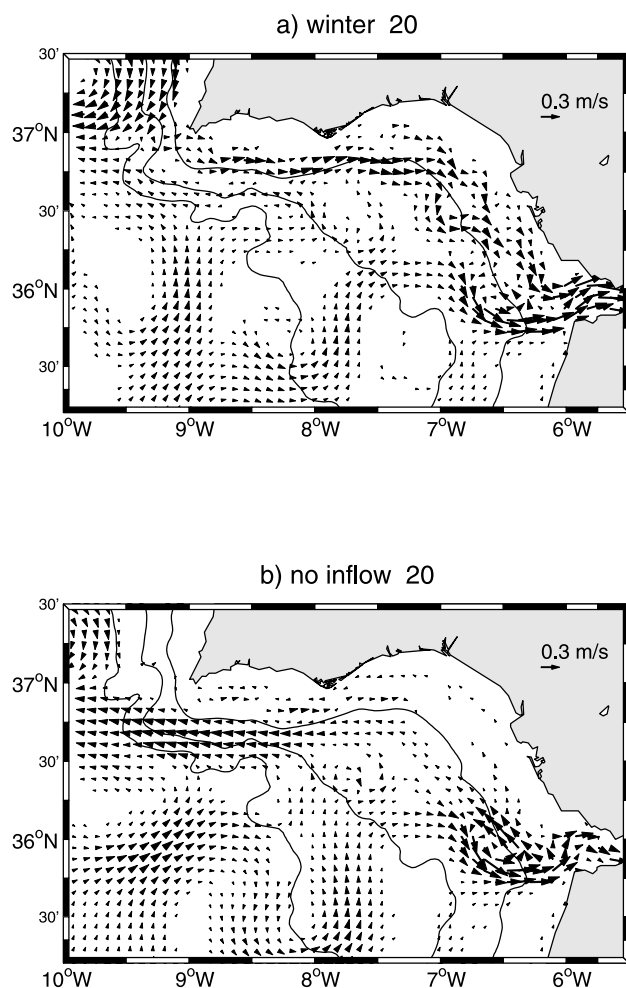
a) winter 20

b) no inflow 20

Figure 17. Comparison of time-mean surface flow vectors (same as Figure 16), except for: (a) winter and (b) the experiment with no inflow from the Atlantic into the Mediterranean Sea.

needed 0.7 Sv, a persistent secondary flow, that we termed Gulf of Cadiz Slope Current, develops along the northern upper slope to complement the Atlantic inflow.

7. Discussion

7.1. Model Limitations

[52] The entrainment of Central Water by the descending Mediterranean overflow is the main forcing of the ocean circulation in the eastern Gulf of Cadiz. However, the entrainment in itself is poorly known as a process, and is strongly dependent on details of mixing that are difficult to measure [e.g., *Baringer and Price*, 1997a, 1997b]. Mixing occurs in the bottom boundary layer forced by bottom friction, and along the interface between the denser Mediterranean outflow water and the overlying Atlantic Central Water. The interface between these two layers is prone to Kelvin-Helmholtz instabilities which are responsible for the bulk of the entrainment [*Baringer and Price*, 1997a; *Mauritzen et al.*, 2001]. Since the present model is hydrostatic, the vertical mixing is parameterized and these mixing details are only marginally resolved. With the

purpose of obtaining realistic values of density along the Mediterranean Undercurrent, a point of enhanced horizontal mixing is added in the zone off the Gibraltar Strait where most of the mixing and entrainment is produced. The resulting Mediterranean Undercurrent temperature and salinity are within the observed values (although saltier in some cases) and the progression of the plume downslope matches the observations. However, all the details of the water masses are not fully reproduced, and the lateral development of the multiple core salinity structure is not clearly perceptible in the model.

7.2. The β Plume and the Azores Current

[53] Our modeling results using high-resolution nested grids with explicit representation of the exchange between the Mediterranean Sea and the Atlantic, confirm the theoretical predictions and simplified models of *Kida* [2006]. A time mean cyclonic cell with transports of about 4 Sv is generated from the Gulf of Cadiz westward. The cyclonic cell resembles the topographic and eddy-driven β plumes of *Kida* [2006]. The β plume in the present model is constituted by a slow and broad flow from the southwest that is transformed into a westward slope jet intensified at intermediate depths along with the Mediterranean Undercurrent. The trapping of offshore flow to the slope occurs at the slope zone between the southern edge of the Strait and the southwest of Cape St. Maria. This picture is however, strongly perturbed by a particularly active mesoscale eddy field. In this context, the wide range of values relative to transport estimates from observations (see *Sánchez and Relvas* [2003] for a compilation) is understandable. However, if the effects of the mesoscale eddies are averaged out, the obtained transport value is probably similar to the one estimated in this work. *Paillet and Mercier* [1997] estimate that about 4.5 Sv reach the Gulf of Cadiz in their inverse model based on climatological observations.

[54] Integrating the time-averaged flow down to 1000 m, the transport near the Gulf of Cadiz is over 5 Sv. Nonetheless, this figure is still about half the transport values measured west of Madeira and also simulated in our larger-scale solution. The β-plume model alone do not explain the whole transport of the Azores Current neither the increase in transport toward the west.

[55] On the basis of the validity of equation (1) the westward advection of vorticity may occur within a background vorticity associated with the wind-driven forcing. We hypothesize that the vorticity anomaly generated inside the Gulf of Cadiz (the β plume) is advected westward into a broad wind-driven environment characterized by meridionally aligned streamlines. Assuming that the contributions to the potential vorticity field are independent, and that a linear sum holds, then the final effect is to bend and compress the streamlines of the background flow westward. This simple conceptual mechanism is represented in Figure 18 (compare with stream function of the time-mean flow for the large-scale solution in Figure 5). The resulting flow field is intensified in the west since it is expected that the transport at point A is larger than at point B, even though the β-plume forcing is closer to point B. The convergence in point B could then trigger the frontogenesis and the meandering nature of the AzC [*Spall*, 1997; *Alves*
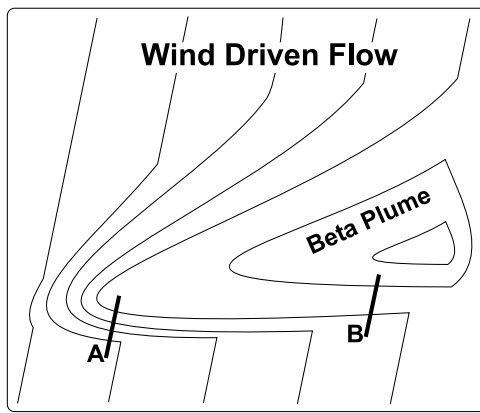
Figure 18. Conceptual scheme of the circulation in the northeastern mid Atlantic. The lines represent the stream lines associated with the basin-scale wind-driven flow deformed by the presence of a β plume. A zonal band of convergence is generated that represents the Azores Current. The transport at section A is larger than at B.

and Colin de Verdière, 1999]. This hypothesis will require a further modeling study in a two-way nesting application.

7.3. Gulf of Cadiz Slope Current

[56] The most robust feature of our numerical results is the very persistent slope current running from the Cape of St. Vincent equatorward into the Strait of Gibraltar. In the mean flow, velocities up to 0.2 m/s are apparent along the upper slope vanishing rapidly around 200 m depth. A small increase toward the Strait is noticed and different values were obtained for the different experiments ranging from 0.3 to 0.5 Sv. Interestingly, in the summer situation, a clear separation of the flow downstream Cape St. Maria is observed. Analysis of SST from this zone show that a cold band usually develops along the northern shelf and upper slope from Caps St. Vincent onward, eventually separating past Cape St. Maria and generating a tongue of cold water oriented southwestward, the "Huelva front" [e.g., *Relvas and Barton*, 2002; *Folkard et al.*, 1997]. The origin of such cold waters was not clear and the authors hypothesized that it was a continuation of the upwelling current from the west coast that contoured the Cape St. Vincent along the shelf, with eventual contributions from local upwelling under episodic westerlies. A first gulf-scale, almost synoptic, coverage with CTD and ADCP is presented by *Garcia-Lafuente et al.* [2006] and *Criado-Aldeanueva et al.* [2006]. The authors report a slope current system with the same extension and vertical structure as the one obtained in our model. *Garcia-Lafuente et al.* [2006] shows a circulation scheme (their Figure 7) summarizing three ADCP synoptic surveys in which the current was measured. In their conceptual scheme, the current is bounded on the shallow side by 2 cyclonic shelf structures, respectively to the west and east of Cape St. Maria. Those are not present in our modeling study since the applied forcing was climatological while the shelf features in the work of *Garcia-Lafuente et al.* [2006] were most probably the interpretation of transient shelf circulation events.

[57] Nevertheless, the current structure and the offshore separation paths indicated in the scheme is most consistent with our model results. The authors indicate the west coast as the origin of the current and hypothesize that the circulation inside the Gulf is anticyclonic, and that the current along the upper slope inside the Gulf is a continuation of the western coast upwelling current. Our model results indicate that this current is independent of the dynamics in the west coast. It is present in the summer and in the winter experiments, and in the case with horizontally homogeneous initialization. The current is absent when the Strait of Gibraltar exchange condition is not imposed. The GCC is mainly forced from the east to complement the necessary transport to feed the Atlantic inflow. The continuation with the west coast flow will depend on whether the flow is equatorward and trapped by the topography since separation at Cape St. Vincent is also a common event [*Relvas and Barton*, 2002].

[58] The double core current that merges near the entrance of the Strait (Figures 16a and 16b at about 6°15′W), has never been reported before either using observations or modeling results. Little evidence of it is present in work by *Baringer and Price* [1997b, Figure 2b], although the authors do not discuss this issue. A possible reason is that most observational effort is trended toward the transport inside the Strait or toward the overflow itself. *Send and Baschek* [2001] show a velocity section of ADCP measurements averaged over a tidal period at about 6°6′W (their Plate 9). In their section, we can observe the MU and the inflow running on top of the offshore edge of the MU as our model MU counterflow described above. However, there is no clear evidence of a second inflow core on the northern part.

[59] The double core structure previously discussed is in the time-averaged flow, whereas the zone of the Strait is highly affected by tides and changing winds, and this feature of the inflow may not be evident in synoptic observations. A deeper study of the Gulf of Cadiz Slope Current and its response to synoptic forcing will be given in a different paper.

8. Conclusions

[60] The results of a numerical model have been presented where the Mediterranean Undercurrent is explicitly resolved in a high-resolution model and the background, larger-scale regional context is maintained through nesting. A three dimensional description of the time-mean flow in the Gulf of Cadiz is presented which conforms to many of the surface observations and studies conducted on the MU.

[61] The model confirms the eastern forcing of the Azores Current, and (1) results of the larger-scale experiments show a very realistic AzC despite the western boundary being climatological; (2) the nested experiments confirm the generation of a time-mean recirculation cyclonic cell like the topographic and eddy-driven β-plume models of *Kida* [2006], and match the transport calculations in inverse models based on climatology [e.g., *Paillet and Mercier*, 1997]; (3) the representation of the Strait of Gibraltar inflow/outflow condition is fundamental to produce a realistic current system in depth, offshore and over the shelf and upper slope; (4) west of Madeira the AzC is not critically

dependent on the details of the entrainment and representation of the Mediterranean Undercurrent since the larger-scale model solution includes the main features observed in nature; and (5) it was hypothesized that the westward increase in the AzC is associated with the coupling between the β plume generated inside the Gulf of Cadiz and the background basin-scale, wind-driven flow. The resulting vorticity field is constituted by a potential vorticity zonal anomaly (forced by the β plume) over the otherwise meridionally aligned large-scale flow field. This hypothesis should however be verified in a two-way nesting model configuration since the mechanism of westward expansion of the β plume is not clear.

[62] At the scale of the Gulf of Cadiz, the current system is dominated offshore by a cyclonic circulation with southwest flow being captured into the slope to feed a westward slope current that is intensified at intermediate depths, showing two sharp cores at about 600 and 1000 m. This whole system recirculating between 4 and 5 Sv. Near the coast the model results show a persistent upper slope current running all the way along the northern part of the Gulf and entering the Strait of Gibraltar. The current is associated with the Strait of Gibraltar inflow/outflow condition, and at times promotes continuity between the southwest Iberian Peninsula and the eastern Gulf of Cadiz. The current eventually separates east of the Cape St. Maria, and generates offshore fronts recurrent in infrared satellite imagery. Since this feature is frequently observed, and since it constitutes the most conspicuous feature of the model results after the Mediterranean Undercurrent, we suggest that it be referred to as the Gulf of Cadiz slope Current. No strong seasonal changes were apparent in the model results but the system is strongly perturbed by the mesoscale eddy field.

References

Alves, M., and A. Colin de Verdière (1999), Instability dynamics of a subtropical jet and applications to the azores front current system: Eddy-driven mean flow, *J. Phys. Oceanogr.*, *29*(5), 837–864.

Ambar, I., and M. Howe (1979), Observations of the Mediterranean outflow: I. mixing in the Mediterranean outflow, *Deep Sea Res., Part A*, *26*, 535–554.

Arhan, M., A. Colin de Verdière, and L. Mémery (1994), The eastern boundary of the subtropical North Atlantic, *J. Phys. Oceanogr.*, *24*, 1295–1316.

Baringer, M., and J. Price (1997a), Mixing and spreading of the Mediterranean outflow, *J. Phys. Oceanogr.*, *27*, 1654–1677.

Baringer, M., and J. Price (1997b), Momentum and energy balance of the Mediterranean outflow, *J. Phys. Oceanogr.*, *27*, 1678–1692.

Baschek, B., U. Send, J. Lafuente, and J. Candela (2001), Transport estimates in the Strait of Gibraltar with a tidal inverse model, *J. Geophys. Res.*, *106*(C12), 31,033–31,044.

Borenas, K., A. Wahlin, I. Ambar, and N. Serra (2002), The Mediterranean outflow splitting—A comparison between theoretical models and CANIGO data, *Deep Sea Res., Part II*, *49*, 4195–4205.

Bower, A., L. Armi, and I. Ambar (1997), Lagrangian observations of Meddy formation during A Mediterranean Undercurrent Seeding Experiment, *J. Phys. Oceanogr.*, *27*, 2445–2575.

Carton, X., L. Chérubin, J. Paillet, Y. Morel, A. Serpette, and B. Le Cann (2002), Meddy coupling with a deep cyclone in the Gulf of Cadiz, *J. Mar. Syst.*, *32*(1–3), 13–42.

Criado-Aldeanueva, F., J. Garcia-Lafuente, J. M. Vargas, J. Del Rio, A. Vazquez, A. Reul, and A. Sanchez (2006), Distribution and circulation of water masses in the Gulf of Cadiz from in situ observations, *Deep Sea Res., Part II*, *53*, 1144–1160.

da Silva, A., A. C. Young, and S. Levitus (1994), *Atlas of Surface Marine Data 1994*, vol. 1, *Algorithms and Procedures*, NOAA Atlas NESDIS 6, NOAA, Silver Spring, Md.

Folkard, A., P. Davies, A. Fiúza, and I. Ambar (1997), Remotely sensed sea surface thermal patterns in the Gulf of Cadiz and the Strait of Gibraltar: Variability, correlations, and relationships with the surface wind field, *J. Geophys. Res.*, *102*(C3), 5669–5683.

Garcia-Lafuente, J., J. Delgado, F. Criado-Aldeanueva, M. Bruno, J. del Rio, and J. Miguel Vargas (2006), Water mass circulation on the continental shelf of the Gulf of Cadiz, *Deep Sea Res., Part II*, *53*, 1182–1197.

Haidvogel, D., and A. Beckmann (1999), *Numerical Ocean Circulation Modeling*, Imperial College Press, London.

Jia, Y. (2000), Formation of an Azores Current due to mediterranean overflow in a modeling study of the North Atlantic, *J. Phys. Oceanogr.*, *30*, 2342–2358.

Kida, S. (2006), Overflows and upper ocean interaction: A mechanism for the Azores Current, Ph.D. thesis, Woods Hole Oceanogr. Inst./Mass. Inst. of Technol., Cambridge, Mass. (Available at http://web.mit.edu/kida/Public/kida-Sept2006-PhDthesis.pdf)

Large, W., J. McWilliams, and S. Doney (1994), Oceanic vertical mixing: A review and model with a nonlocal boundary layer parameterization, *Rev. Geophys.*, *32*(4), 363–403.

Levitus, S., and T. Boyer (1994), *World Ocean Atlas 1994*, vol. 4, *Temperature*, NOAA Atlas NESDIS 4, NOAA, Silver Spring, Md.

Levitus, S., R. Burgett, and T. Boyer (1994), *World Ocean Atlas 1994*, vol. 3, *Salinity*, NOAA Atlas NESDIS 3, NOAA, Silver Spring, Md.

Lumpkin, R., and S. L. Garzoli (2005), Near-surface circulation in the tropical Atlantic Ocean, *Deep Sea Res., Part I*, *52*, 495–518.

Marchesiello, P., J. C. McWilliams, and A. F. Shchepetkin (2001), Open boundary conditions for long-term integration of regional oceanic models, *Ocean Modell.*, *3*, 1–20.

Marchesiello, P., J. McWilliams, and A. Shchepetkin (2003), Equilibrium structure and dynamics of the california current system, *J. Phys. Oceanogr.*, *33*, 753–783.

Mauritzen, C., Y. Morel, and J. Paillet (2001), On the influence of Mediterranean water on the central waters of the North Atlantic Ocean, *Deep Sea Res., Part I*, *48*, 347–381.

Özgökmen, T., E. Chassignet, and C. Rooth (2001), On the connection between the Mediterranean outflow and the Azores Current, *J. Phys. Oceanogr.*, *31*, 461–480.

Paillet, J., and H. Mercier (1997), An inverse model of the eastern North Atlantic general circulation and thermocline ventilation, *Deep Sea Res., Part I*, *44*, 1293–1328.

Papadakis, M., E. P. Chassignet, and R. W. Hallberg (2003), Numerical simulations of the mediterranean sea outflow: Impact of the entrainment parameterization, *Ocean Modell.*, *5*, 325–356.

Pedlosky, J. (1997), *Ocean Circulation Theory*, Springer, New York.

Peliz, A., J. Dubert, A. Santos, P. Oliveira, and B. Le Cann (2005), Winter upper ocean circulation in the Western Iberian Basin—Fronts, eddies and poleward flows: An overview, *Deep Sea Res., Part I*, *52*, 621–646.

Penven, P. (2003), ROMTOOLS user's guide, technical report, Inst. de Rech. pour le Dev., Paris.

Penven, P., J. Echevin, J. Pasapera, F. Colas, and J. Tam (2005), Average circulation, seasonal cycle, and mesoscale dynamics of the Peru Current System: A modeling approach, *J. Geophys. Res.*, *110*, C10021, doi:10.1029/2005JC002945.

Penven, P., L. Debreu, P. Marchesiello, and J. McWilliams (2006), Evaluation and application of the ROMS 1-way embedding procedure to the Central California Upwelling System, *Ocean Modell.*, *12*, 157–187.

Relvas, P., and E. Barton (2002), Mesoscale patterns in the Cape São Vicente (Iberian Peninsula) upwelling region, *J. Geophys. Res.*, *107*(C10), 3164, doi:10.1029/2000JC000456.

Relvas, P., and E. Barton (2005), A separated jet and coastal counterflow during upwelling relaxation off Cape São Vicente (Iberian Peninsula), *Cont. Shelf Res.*, *25*, 29–49.

Sánchez, R., and P. Relvas (2003), Spring-summer climatological circulation in the upper layer in the region of Cape St. Vincent, Southest Portugal, *ICES J. Mar. Sci.*, *60*, 1232–1250, doi:10.1016/S1054-3139(03)00137-1.

Sánchez, R., E. Mason, P. Relvas, A. da Silva, and A. Peliz (2006), On the inshore circulation in the northern Gulf of Cadiz, southern Portuguese shelf, *Deep Sea Res., Part II*, *53*, 1198–1218.

Send, U., and B. Baschek (2001), Intensive shipboard observatios of the flow through the Strait of Gibraltar, *J. Geophys. Res.*, *106*(C12), 31,017–31,032.

Serra, N., and I. Ambar (2002), Eddy generation in the Mediterranean undercurrent, *Deep Sea Res., Part II*, *49*, 4225–4243.

Serra, N., I. Ambar, and R. Käse (2005), Observations and numerical modelling of the Mediterranean outflow splitting and eddy generation, *Deep Sea Res., Part II*, *52*, 383–408.

Shchepetkin, A. F., and J. C. McWilliams (2003), A method for computing horizontal pressure-gradient force in an oceanic model with a nonaligned vertical coordinate, *J. Geophys. Res.*, *108*(C3), 3090, doi:10.1029/2001JC001047.

Shchepetkin, A. F., and J. C. McWilliams (2005), The regional oceanic modeling system (ROMS): A split-explicit, free-surface, topography-following-coordinate oceanic model, *Ocean Modell.*, *9*, 347–404.

Smith, W., and D. Sandwell (1997), Global sea floor topography from satellite altimetry and ship depth soundings, *Science*, *277*(5334), 1956–1962, doi:10.1126/science.277.5334.1956.

Spall, M. (1997), Baroclinic jets in confluent flow, *J. Phys. Oceanogr.*, *27*, 1054–1071.

Stommel, H. (1982), Is the South Pacific helium-3 plume dynamically active?, *Earth Planet. Sci. Lett.*, *61*, 63–67.

Tsimplis, M., and H. Bryden (2000), Estimation of the transports through the Strait of Gibraltar, *Deep Sea Res., Part I*, *47*, 2219–2242, doi:10.1016/S0967-0637(00)00024-8.

_____

J. Dubert, A. Peliz, and A. Teles-Machado, Departamento de Fisica, Universidade de Aveiro, 3810-193 Aveiro, Portugal. (apeliz@fis.ua.pt)

P. Marchesiello, Institut de Recherche pour le Développement, 101 Promenade Roger Laroque, BP A5-98848 Noumea, New Caledonia.